

# $K \rightarrow 3\pi$ Final State Interactions at NLO in CHPT and Cabibbo's Proposal to Measure $a_0 - a_2$

---

**Elvira Gámiz**

*Department of Physics and Astronomy, The University of Glasgow, Glasgow G12 8QQ,  
United Kingdom*

**Joaquim Prades**

*CAFPE and Departamento de Física Teórica y del Cosmos, Universidad de Granada,  
Campus de Fuente Nueva, E-18002 Granada, Spain*

**Ignazio Scimemi**

*Departament de Física Teòrica, IFIC, CSIC-Universitat de València,  
Apt. de Correus 22085, E-46071 València, Spain*

**ABSTRACT:** We present the analytical results for the  $K \rightarrow 3\pi$  final state interactions at next-to-leading order (NLO) in CHPT. We also study the recent Cabibbo's proposal to measure the  $\pi\pi$  scattering lengths combination  $a_0 - a_2$  from the cusp effect in the  $\pi^0\pi^0$  energy spectrum at threshold for  $K^+ \rightarrow \pi^0\pi^0\pi^+$  and  $K_L \rightarrow \pi^0\pi^0\pi^0$ , and give the relevant formulas to describe it at NLO. For that, we use the NLO CHPT expression to fit the real part of  $K \rightarrow 3\pi$  to data while the  $\pi\pi$  scattering lengths are treated non-perturbatively. Using them, we make a quantitative estimate of the theoretical uncertainty of the  $a_0 - a_2$  determination at NLO in our approach and obtain that it is not smaller than 5 % if added quadratically and 7 % if linearly for  $K^+ \rightarrow \pi^0\pi^0\pi^+$ . One gets similar theoretical uncertainties if the neutral  $K_L \rightarrow \pi^0\pi^0\pi^0$  decay data below threshold are used instead. For this decay, there are very large theoretical uncertainties above threshold due to cancellations and data above threshold cannot be used to get the scattering lengths. All the numbers we present are in the isospin limit apart of two-pion phase space factors which are physical. We compare our results for the cusp effect with Cabibbo and Isidori's results and discuss the differences and agreements. We also comment on the appearance of the singularity at the  $K \rightarrow 3\pi$  pseudo-threshold  $s = (m_K - m_\pi)^2$  in the discontinuity that defines the cusp.

**KEYWORDS:** Kaon Physics, Chiral Lagrangians, QCD.

---

## Contents

<b>1. Introduction</b>	<b>1</b>
<b>2. Notation</b>	<b>3</b>
<b>3. FSI for <math>K \rightarrow 3\pi</math> at NLO</b>	<b>5</b>
<b>4. Cabibbo's Proposal at NLO in CHPT</b>	<b>6</b>
4.1 Cabibbo's Proposal for Charged Kaon Decays	9
4.2 Cabibbo's Proposal for Neutral Kaons	16
<b>5. Summary and Conclusions</b>	<b>21</b>
<b>A. Numerical Inputs</b>	<b>23</b>
<b>B. FSI at NLO for Neutral Kaon Decays: Two-Pion Cuts</b>	<b>24</b>
B.1 Notation	24
B.2 FSI for $K_L \rightarrow \pi^0\pi^0\pi^0$ at NLO	25
B.3 FSI for $K_L \rightarrow \pi^+\pi^-\pi^0$ at NLO	26
B.4 FSI for $K_S \rightarrow \pi^+\pi^-\pi^0$ at NLO	27
<b>C. Three-Pion Cut Contributions to FSI</b>	<b>28</b>

---

## 1. Introduction

Final state interactions (FSI) at next-to-leading order (NLO) in Chiral Perturbation Theory<sup>1</sup> (CHPT) [3, 4] are needed to obtain the charged CP-violating asymmetries at NLO [5, 6, 7]. The dominant contribution to these  $K^+ \rightarrow 3\pi$  FSI at NLO are from two-pion cuts for topology A in Figure 1. They were calculated analytically in [5].

Though to get the full  $K \rightarrow 3\pi$  amplitudes at order  $p^6$  implies a two-loop calculation, one can get the FSI at NLO using the optical theorem within CHPT with the advantage that one just needs to know  $\pi\pi$  scattering and  $K \rightarrow 3\pi$  both at  $\mathcal{O}(p^4)$ . Notice that NLO in the dispersive part of the amplitude means one-loop and  $\mathcal{O}(p^4)$  in CHPT while NLO in the absorptive part of the amplitude means two-loops and  $\mathcal{O}(p^6)$  in CHPT.

In [5], we took the  $\pi\pi$  scattering results from [8] and calculated the amplitudes  $K \rightarrow 3\pi$  at NLO in the isospin limit. We agreed with the NLO  $K \rightarrow 3\pi$  results recently published in [9]. These were previously calculated in [10] and used in [11], but unfortunately the analytical full results were not available there. Now, there is also available the full one-loop

---

<sup>1</sup>Some introductory lectures on CHPT can be found in [1] and recent reviews in [2].

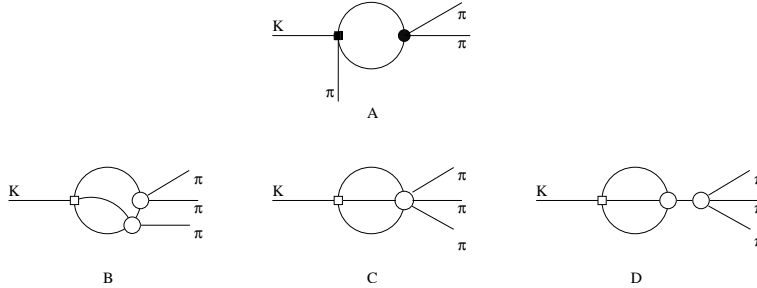


**Figure 1:** Some topologies contributing to the FSI in  $K \rightarrow 3\pi$  decays at LO and NLO. The square is the weak vertex and the circle is the strong one. In topology A, solid circles include both tree and one-loop level vertices.

$K \rightarrow 3\pi$  amplitudes including isospin breaking effects from quark masses and electromagnetic interactions [12, 13].

In the meantime, we discovered some small errata in the published formulas in [5] which were corrected in [6]. We correct here another erratum in Eqs. (6.6), (6.7) and (6.9) in [5] where we wrote  $\mathbb{R}$  instead of  $\widetilde{\mathbb{R}}$ . See Section 3 in the present work for the correction. In addition, the matrix elements 21 and 22 in Eqs. (6.7) and (6.9) in [5] were interchanged. None of these errata affects the results for the CP-violating asymmetries nor the conclusions given in [5, 6, 7].

The details of the use of the optical theorem to calculate the two-pion cut contributions from topology A in Figure 1—solid circles include both tree and one-loop level vertices—were given in Appendix E of the first reference in [5]. Notice that two-pion cuts of topology B are already included in topology A when one takes the weak vertex at one-loop. We don't repeat them now.

Here, we complete the calculation of these FSI by evaluating the three-pion cuts in topologies B, C and D in Figure 1 for  $K^+ \rightarrow 3\pi$ . We also provide with the neutral kaon  $K_{L,S} \rightarrow 3\pi$  final state interactions at  $\mathcal{O}(p^6)$  including both two- and three-pion cut contributions. Thus, we give the full  $K \rightarrow 3\pi$  FSI at NLO in CHPT in the isospin limit for all  $K \rightarrow 3\pi$  decays.

The study of FSI in  $K \rightarrow 3\pi$  at two-loops also became of relevance after the proposal by Cabibbo [14] to measure the combination  $a_0 - a_2$  of  $\pi\pi$  scattering lengths using the cusp effect in the  $\pi^0\pi^0$  spectrum at threshold in  $K^+ \rightarrow \pi^0\pi^0\pi^+$  and  $K_L \rightarrow \pi^0\pi^0\pi^0$  decay rates<sup>2</sup>. Within this proposal, it has been recently presented in [16] the effects of FSI at NLO using formulas dictated by unitarity and analyticity approximated at second order in the  $\pi\pi$  scattering lengths,  $a_i \sim 0.2$ . The error was therefore canonically assumed to be of order of  $a_i^2$ , i.e., 5%. It is of interest to check this canonical error and provide a complementary analysis of the theoretical uncertainty. We use our NLO in CHPT results for the form of the real part of  $K \rightarrow 3\pi$  which has to be fitted to data to give the formulas of the cusp effect always leaving the  $\pi\pi$  scattering near threshold as in Cabibbo's original proposal. The advantage of using CHPT is that it contains the correct singularity structure at NLO

<sup>2</sup>The cusp effect in SU(2)  $\pi\pi$  scattering was discussed in [15].

in CHPT which can be systematically improved in an effective field theory framework by going at higher orders.

Contributions from next-to-next-to-leading order (NNLO)  $SU(3)$  CHPT in the isospin limit are expected typically to be around  $(3 \sim 5)\%$ , so that our NLO results are just a first step in order to reduce the theoretical error on the determination of the combination  $a_0 - a_2$  to the few per cent level. Once the isospin limit NNLO CHPT contribution is eventually evaluated, one can follow the procedure that we use here to get a more accurate measurement of  $a_0 - a_2$  and check the assumed NNLO uncertainty. At that point, and in order to reach the few per cent level in the theoretical uncertainty, it will be necessary to include full isospin breaking effects at NLO too. These are also expected to be of a few per cent as was found for  $K \rightarrow 3\pi$  in [12, 13].

In Sections 2 and 3 we introduce the needed notation in the description of  $K \rightarrow 3\pi$  in CHPT and the final state interactions at NLO, respectively. In Section 4 we give the relevant formulas using our NLO results for the singularity structure of the real part of  $K \rightarrow 3\pi$  to be used in a fit of the experimental  $K \rightarrow 3\pi$  cusp effect to data to extract the  $a_0 - a_2$  phase shift combination. We compare our results with the ones in [16] and give estimates of the theoretical uncertainties in the determination of  $a_0 - a_2$ . We do this both for  $K^+ \rightarrow \pi^0 \pi^0 \pi^+$  and for  $K_L \rightarrow \pi^0 \pi^0 \pi^0$ . We would like to advance here that our analytical results agree fully with those in [16] if we make the same approximations. Finally, we summarize our results and main conclusions in Section 5.

In Appendix A we list the numerical inputs used. In Appendix B we present the FSI results for the neutral kaon  $K \rightarrow 3\pi$  decays from two-pion cuts contributions from topology A in Figure 1. Finally, in Appendix C we collect the results for all three-pion cut contributions from topologies B, C, and D in Figure 1.

## 2. Notation

Here, we want to give the basic notation that we use in the following. In [5] we calculated the amplitudes with  $K_{1(2)} \equiv (K^0 - (+)\overline{K^0})/\sqrt{2}$ ,

$$\begin{aligned} K_2(k) &\rightarrow \pi^0(p_1)\pi^0(p_2)\pi^0(p_3), \quad [A_{000}^2], \\ K_2(k) &\rightarrow \pi^+(p_1)\pi^-(p_2)\pi^0(p_3), \quad [A_{+-0}^2], \\ K_1(k) &\rightarrow \pi^+(p_1)\pi^-(p_2)\pi^0(p_3), \quad [A_{+-0}^1], \\ K^+(k) &\rightarrow \pi^0(p_1)\pi^0(p_2)\pi^+(p_3), \quad [A_{00+}], \\ K^+(k) &\rightarrow \pi^+(p_1)\pi^+(p_2)\pi^-(p_3), \quad [A_{++-}], \end{aligned} \quad (2.1)$$

as well as their CP-conjugated decays at NLO (i.e. order  $p^4$  in this case) in the chiral expansion and in the isospin symmetry limit  $m_u = m_d$ . Disregarding CP-violating effects, that are negligible in the results reported in this work,  $K_1 \simeq K_S$  and  $K_2 \simeq K_L$ .

The lowest order  $SU(3) \times SU(3)$  chiral Lagrangian describing  $|\Delta S| = 1$  transitions is

$$\begin{aligned} \mathcal{L}_{|\Delta S|=1}^{(2)} = & C F_0^6 e^2 G_E \text{tr} \left( \Delta_{32} u^\dagger Q u \right) + C F_0^4 \left[ G_8 \text{tr} \left( \Delta_{32} u_\mu u^\mu \right) + G'_8 \text{tr} \left( \Delta_{32} \chi_+ \right) \right. \\ & \left. + G_{27} t^{ij,kl} \text{tr} \left( \Delta_{ij} u_\mu \right) \text{tr} \left( \Delta_{kl} u^\mu \right) \right] + \text{h.c.} \end{aligned} \quad (2.2)$$

with

$$C = -\frac{3}{5} \frac{G_F}{\sqrt{2}} V_{ud} V_{us}^* \simeq -1.07 \times 10^{-6} \text{ GeV}^{-2}. \quad (2.3)$$

The correspondence with the couplings  $c_2$  and  $c_3$  of [10] is

$$\begin{aligned} c_2 &= C F_0^4 G_8; \\ c_3 &= -\frac{1}{6} C F_0^4 G_{27}. \end{aligned} \quad (2.4)$$

$F_0$  is the chiral limit value of the pion decay constant  $f_\pi = (92.4 \pm 0.4)$  MeV,

$$\begin{aligned} u_\mu &\equiv i u^\dagger (D_\mu U) u^\dagger = u_\mu^\dagger, \\ \Delta_{ij} &= u \lambda_{ij} u^\dagger (\lambda_{ij})_{ab} \equiv \delta_{ia} \delta_{jb}, \\ \chi_{+(-)} &= u^\dagger \chi u^\dagger + (-) u \chi^\dagger u \end{aligned} \quad (2.5)$$

$\chi = \text{diag}(m_u, m_d, m_s)$  is a  $3 \times 3$  matrix collecting the light quark masses,  $U \equiv u^2 = \exp(i\sqrt{2}\Phi/F_0)$  is the exponential representation incorporating the octet of light pseudo-scalar mesons in the SU(3) matrix  $\Phi$ ;

$$\Phi \equiv \begin{pmatrix} \frac{\pi^0}{\sqrt{2}} + \frac{\eta_8}{\sqrt{6}} & \pi^+ & K^+ \\ \pi^- & -\frac{\pi^0}{\sqrt{2}} + \frac{\eta_8}{\sqrt{6}} & K^0 \\ K^- & \bar{K}^0 & -2 \frac{\eta_8}{\sqrt{6}} \end{pmatrix}.$$

The non-zero components of the  $\text{SU}(3) \times \text{SU}(3)$  tensor  $t^{ij,kl}$  are

$$\begin{aligned} t^{21,13} &= t^{13,21} = \frac{1}{3}; & t^{22,23} &= t^{23,22} = -\frac{1}{6}; \\ t^{23,33} &= t^{33,23} = -\frac{1}{6}; & t^{23,11} &= t^{11,23} = \frac{1}{3}; \end{aligned} \quad (2.6)$$

and  $Q = \text{diag}(2/3, -1/3, -1/3)$  is a  $3 \times 3$  matrix which collects the electric charge of the three light quark flavors.

Making use of the Dalitz variables

$$x \equiv \frac{s_1 - s_2}{m_{\pi^+}^2} \quad \text{and} \quad y \equiv \frac{s_3 - s_0}{m_{\pi^+}^2} \quad (2.7)$$

with  $s_i \equiv (k - p_i)^2$ ,  $3s_0 \equiv m_K^2 + m_{\pi^{(1)}}^2 + m_{\pi^{(2)}}^2 + m_{\pi^{(3)}}^2$ , the amplitudes in (2.1) [without isospin breaking terms] can be written as expansions in powers of  $x$  and  $y$

$$\begin{aligned} A_{+-} &= (-2\alpha_1 + \alpha_3) - (\beta_1 - \frac{1}{2}\beta_3 + \sqrt{3}\gamma_3) y + \mathcal{O}(y^2, x), \\ A_{00+} &= \frac{1}{2}(-2\alpha_1 + \alpha_3) - (-\beta_1 + \frac{1}{2}\beta_3 + \sqrt{3}\gamma_3) y + \mathcal{O}(y^2, x), \\ A_{+-0}^2 &= (\alpha_1 + \alpha_3)^R - (\beta_1 + \beta_3)^R y + \mathcal{O}(y^2, x), \\ A_{+-0}^1 &= (\alpha_1 + \alpha_3)^I - (\beta_1 + \beta_3)^I y + \mathcal{O}(y^2, x), \\ A_{000}^2 &= 3(\alpha_1 + \alpha_3)^R + \mathcal{O}(y^2, x), \\ A_{000}^1 &= 3(\alpha_1 + \alpha_3)^I + \mathcal{O}(y^2, x), \end{aligned} \quad (2.8)$$

where the parameters  $\alpha_i$ ,  $\beta_i$  and  $\gamma_i$  are functions of the pion and kaon masses,  $F_0$ , the lowest order  $\Delta S = 1$  Lagrangian couplings  $G_8$ ,  $G'_8$ ,  $G_{27}$ ,  $G_E$  and the counterterms appearing at order  $p^4$ , i.e.,  $L'_i$ s and  $\tilde{K}'_i$ s. The definition of these last ones can be found in Section 3.2 of [5]. In (2.8), super-indices  $R$  and  $I$  mean that either the real or the imaginary part of the counterterms appear.

If we do not consider FSI, the complex parameters  $\alpha_i$ ,  $\beta_i$  and  $\gamma_i$  can be written at NLO in terms of the order  $p^2$  and  $p^4$  counterterms and the constants  $B_{i,0(1)} = B_{i,0(1)}^{(2)} + B_{i,0(1)}^{(4)}$  and  $H_{i,0(1)}^{(4)}$  defined in Appendix B of [5]. There, we gave  $\alpha_i$ ,  $\beta_i$  and  $\gamma_i$  at LO in CHPT as well as their analytic expressions at NLO.

### 3. FSI for $K \rightarrow 3\pi$ at NLO

The strong FSI mix the two final states with isospin  $I = 1$  and leave unmixed the isospin  $I = 2$  state. The mixing in the isospin  $I = 1$  decay amplitudes is taken into account by introducing the strong re-scattering  $2 \times 2$  matrix  $\mathbb{R}$ . The amplitudes in (2.1) including the FSI effects can be written at all orders, in the isospin symmetry limit, as follows [17],

$$\begin{aligned} T_c \begin{pmatrix} A_{++-}^{(I=1)} \\ A_{00+}^{(I=1)} \end{pmatrix}_{\text{Res}} &= (\mathbb{I} + i\mathbb{R}) T_c \begin{pmatrix} A_{++-}^{(I=1)} \\ A_{00+}^{(I=1)} \end{pmatrix}_{\text{NRes}}, \\ T_n \begin{pmatrix} A_{+-0}^2 \\ A_{000}^2 \end{pmatrix}_{\text{Res}} &= (\mathbb{I} + i\mathbb{R}) T_n \begin{pmatrix} A_{+-0}^2 \\ A_{000}^2 \end{pmatrix}_{\text{NRes}}, \\ A_{++-}^{(I=2)}|_{\text{Res}} &= (1 + i\delta_2) A_{++-}^{(I=2)}|_{\text{NRes}}, \end{aligned} \quad (3.1)$$

with the matrices

$$T_c = \frac{1}{3} \begin{pmatrix} 1 & 1 \\ 1 & -2 \end{pmatrix}, \quad T_n = \frac{1}{3} \begin{pmatrix} 0 & 1 \\ -3 & 1 \end{pmatrix} \quad (3.2)$$

projecting the final state with  $I = 1$  into the symmetric–non-symmetric basis [17]. The subscript Res (NRes) in (3.1) means that the re-scattering effects have (not) been included. In these definitions, the matrix  $\mathbb{R}$ ,  $\delta_2$  and the amplitudes  $A^{(i)}$  depend on  $s_1$ ,  $s_2$  and  $s_3$ .

Using the usual isospin decomposition of  $K \rightarrow 3\pi$  amplitudes in the isospin limit

$$\begin{aligned} A_{++-}(s_1, s_2, s_3) &= 2A_c(s_1, s_2, s_3) + B_c(s_1, s_2, s_3) + B_t(s_1, s_2, s_3), \\ A_{00+}(s_1, s_2, s_3) &= A_c(s_1, s_2, s_3) - B_c(s_1, s_2, s_3) + B_t(s_1, s_2, s_3), \\ A_{+-0}(s_1, s_2, s_3) &= C_0(s_1, s_2, s_3) + \frac{2}{3} [B_t(s_3, s_2, s_1) - B_t(s_3, s_1, s_2)] \\ &\quad + A_n(s_1, s_2, s_3) - B_n(s_1, s_2, s_3), \\ A_{000}(s_1, s_2, s_3) &= 3A_n(s_1, s_2, s_3), \end{aligned} \quad (3.3)$$

one finds for the elements of  $\mathbb{R}$ ,

$$\mathbb{R}_{11} = \frac{B_n^{\text{NRes}} \text{Im } A_c - B_c^{\text{NRes}} \text{Im } A_n}{A_c^{\text{NRes}} B_n^{\text{NRes}} - A_n^{\text{NRes}} B_c^{\text{NRes}}},$$

$$\begin{aligned}
\mathbb{R}_{12} &= \frac{A_c^{\text{NRes}} \text{Im } A_n - A_n^{\text{NRes}} \text{Im } A_c}{A_c^{\text{NRes}} B_n^{\text{NRes}} - A_n^{\text{NRes}} B_c^{\text{NRes}}} , \\
\mathbb{R}_{21} &= \frac{B_n^{\text{NRes}} \text{Im } B_c - B_c^{\text{NRes}} \text{Im } B_n}{A_c^{\text{NRes}} B_n^{\text{NRes}} - A_n^{\text{NRes}} B_c^{\text{NRes}}} , \\
\mathbb{R}_{22} &= \frac{A_c^{\text{NRes}} \text{Im } B_n - A_n^{\text{NRes}} \text{Im } B_c}{A_c^{\text{NRes}} B_n^{\text{NRes}} - A_n^{\text{NRes}} B_c^{\text{NRes}}} .
\end{aligned} \tag{3.4}$$

At LO,  $\mathbb{R}_{12} = 0$  due to the fact that the only contributions to  $\text{Im } A_i$  come from  $\pi\pi$  re-scattering. At higher orders there are contributions to  $\text{Im } A_i$  which have different origin and therefore  $\mathbb{R}_{12} \neq 0$ . Notice that the re-scattering matrix  $\mathbb{R}$  depends on energy and at  $\pi\pi$  threshold it changes –this is in fact the cusp effect discussed in the following sections.

As explained in [5], we used the optical theorem to calculate the two-pion cuts contributions to FSI at NLO for the charged kaon decays which are the dominant ones. The analytical result of these contributions for the dispersive part of the amplitudes for  $K^+ \rightarrow 3\pi$  can be found in Appendix E of the first reference in [5]. Here, we also calculate analytically these contributions to FSI at NLO for all  $K_{L,S} \rightarrow 3\pi$  and include the three-pion cut contributions in topologies B and C in Figure 1 in all cases. These last three-pion cut contributions have been evaluated numerically –see Appendix C.

The calculation has been done in the isospin limit, apart of the kinematical factors in the optical theorem which are taken physical. This constitutes the first full calculation of FSI in  $K \rightarrow 3\pi$  decays at NLO in CHPT. The results for the dispersive part of the amplitudes for  $K_{L,S} \rightarrow 3\pi$  can be found in Appendix B for two-pion cuts and in Appendix C for three-pion cuts for both neutral and charged  $K \rightarrow 3\pi$ . For the numerical applications in the rest of the paper, we use the inputs in Appendix A.

Equations (3.1) imply the following relation for the two first coefficients of the expansion in powers of  $x$  and  $y$  of the amplitudes in (2.8)

$$\begin{aligned}
\begin{pmatrix} -\alpha_1 + \frac{1}{2}\alpha_3 \\ -\beta_1 + \frac{1}{2}\beta_3 \end{pmatrix}_{\text{Res}} &= (\mathbb{I} + i\tilde{\mathbb{R}}) \begin{pmatrix} -\alpha_1 + \frac{1}{2}\alpha_3 \\ -\beta_1 + \frac{1}{2}\beta_3 \end{pmatrix}_{\text{NRes}} , \\
\begin{pmatrix} \alpha_1 + \alpha_3 \\ \beta_1 + \beta_3 \end{pmatrix}_{\text{Res}} &= (\mathbb{I} + i\tilde{\mathbb{R}}) \begin{pmatrix} \alpha_1 + \alpha_3 \\ \beta_1 + \beta_3 \end{pmatrix}_{\text{NRes}} , \\
\gamma_{3,\text{Res}} &= (1 + i\delta_2) \gamma_{3,\text{NRes}} .
\end{aligned} \tag{3.5}$$

The matrix  $\tilde{\mathbb{R}}$  and the phase  $\delta_2$  were given at LO in [5]. We also gave there the two combinations of the  $\tilde{\mathbb{R}}$  matrix elements that can be obtained from the charged kaon decays. As we already said in the Introduction, there is an erratum in Eqs. (6.6), (6.7) and (6.9) in [5] where we wrote  $\mathbb{R}$  instead of  $\tilde{\mathbb{R}}$ . In addition, in Eqs. (6.7) and (6.9) the matrix elements 21 and 22 were interchanged.

#### 4. Cabibbo's Proposal at NLO in CHPT

Recently, Cabibbo [14] showed that the cusp effect in the total energy spectrum of the

$\pi^0\pi^0$  pair in  $K^+ \rightarrow \pi^0\pi^0\pi^+$  is proportional to the scattering lengths combination  $a_0 - a_2$  and proposed to use this effect to measure it.

This interesting proposal was done at lowest order in the sense that the author just considered topologies of type A in Figure 1. It has been followed up by a study of higher order re-scattering effects coming from topology B in Figure 1 [16]. The first experimental analysis applying this proposal has been already published in [18] showing clearly that the nominal 5 % theoretical accuracy quoted in [16] will dominate this determination. It is therefore very important to check this 5% theoretical uncertainty and how to reduce it further.

In [16], in order to make a quantitative evaluation for the Cabibbo's proposal uncertainties, a power counting in the scattering lengths  $a_i$  was done. The main conclusion was that one needs to include topology B in Figure 1 to go to  $\mathcal{O}(a^2)$  accuracy, i.e. around 5%. The authors used Feynman diagrammatics to do the counting in powers of  $a_i$  although they did not have an effective field theory supporting it. It is of course interesting to construct it and follow that program. In fact, very recently, such an effective field theory has been presented [19]. In [14, 16], the real part of the  $K \rightarrow 3\pi$  amplitude was approximated by a second order polynomial in the relevant final two-pion invariant energy which is fitted to data. We believe that it is also interesting to study the Cabibbo's proposal using the exact form at NLO in CHPT for the real part of  $K \rightarrow 3\pi$  also fitted to data. We present this analysis below. We anticipate that our proposal uses exact NLO CHPT results but is not just full CHPT at that order. In that respect, it is a variation of the original Cabibbo's proposal that uses NLO CHPT for the real part of  $K \rightarrow 3\pi$  vertex instead of the polynomial approximation used in [14, 16] plus analyticity and unitarity.

The cusp effect originates in the different contributions of  $\pi\pi$  scattering to the  $K^+ \rightarrow \pi^0\pi^0\pi^+$  and  $K_L \rightarrow \pi^0\pi^0\pi^0$  amplitudes above and below threshold of  $\pi^+\pi^-$  production. In Section 4.1 for  $K^+ \rightarrow \pi^0\pi^0\pi^+$  and in Section 4.2 for  $K^0 \rightarrow \pi^0\pi^0\pi^0$ , we obtain these contributions using just analyticity and unitarity near threshold, i.e. applying the optical theorem to calculate the imaginary part of the discontinuity across the physical  $\pi^+\pi^-$  cut and Cutkosky rules to calculate the real part of that discontinuity around threshold. In some cases, one can get pieces of the real part of that discontinuity by going below  $\pi^+\pi^-$  threshold. Sometimes this becomes unphysical because the value of the real world pion masses forbids it. In such cases we follow the strategy in [16] of going first to unphysical value of pion masses, e.g.  $m_{\pi^0} > m_{\pi^+}$ , such that the absorptive part below threshold exists and apply the optical theorem in this set up. Then the result is analytically continued above threshold where the amplitude always exists by putting the real value for pion masses.

The explicit application of the optical theorem to  $K \rightarrow 3\pi$  with physical thresholds can be found in [5] and has been used in the previous section. The optical theorem allows to separate the  $\pi\pi$  scattering in the final state interactions, i.e the scattering length effects, from the rest in  $K \rightarrow 3\pi$ . In particular, we introduce the real part of  $\pi\pi$  scattering near threshold non-perturbatively. This means that as the effect of the  $\pi\pi$  scattering must be estimated around threshold, one is intuitively lead to use the scattering length to all orders as a good approximation of  $\pi\pi$  scattering.

Explicitly, we follow [14, 16] for the treatment of  $\pi\pi$  scattering matrix elements near

threshold. At threshold, we use [4]

$$\begin{aligned}
\pi^0\pi^0 \rightarrow \pi^0\pi^0, & \quad \text{Re } A_{00} \equiv 32\pi a_{00} \quad \text{with} \quad a_{00} = \frac{a_0 + 2a_2}{3}, \\
\pi^+\pi^0 \rightarrow \pi^+\pi^0, & \quad \text{Re } A_{+0} \equiv 32\pi a_{+0} \quad \text{with} \quad a_{+0} = \frac{a_2}{2}, \\
\pi^+\pi^- \rightarrow \pi^0\pi^0, & \quad \text{Re } A_x \equiv 32\pi a_x \quad \text{with} \quad a_x = \frac{a_0 - a_2}{3}, \\
\pi^+\pi^- \rightarrow \pi^+\pi^-, & \quad \text{Re } A_{+-} \equiv 32\pi a_{+-} \quad \text{with} \quad a_{+-} = \frac{2a_0 + a_2}{3}, \\
\pi^+\pi^+ \rightarrow \pi^+\pi^+, & \quad \text{Re } A_{++} \equiv 32\pi a_{++} \quad \text{with} \quad a_{++} = a_2, \tag{4.1}
\end{aligned}$$

as a definition of the different effective scattering length combinations measured by fitting the measured cusp effect. We take their expressions in terms of  $a_0$  and  $a_2$  in the isospin conserving limit only as a first approximation. The quantities determined experimentally for these effective scattering lengths combinations should be compared with the CHPT prediction including radiative corrections and isospin breaking [16]. Notice that the scattering lengths are defined at the following thresholds  $s_{th}$ :  $4m_{\pi^+}^2$  for  $a_{00}$ ,  $a_x$ ,  $a_{+-}$  and  $a_{++}$  and  $(m_{\pi^+} + m_{\pi^0})^2$  for  $a_{+0}$ .

In order to describe the  $\pi\pi$  scattering away from threshold one should take into account the kinematical dependence of the amplitudes. Whenever an amplitude is centered around threshold, we follow [16] and perform an expansion in the different kinematical variables on which the amplitudes depend. Up to linear terms, the generic matrix elements –neglecting all higher order but the P wave– are of the form [20]

$$\text{Re } A_{ij} = 32\pi \left[ a_{ij}(s) + \frac{3}{4} a_{ij}^P \frac{(t-u)}{m_{\pi^+}^2} \right] \tag{4.2}$$

with<sup>3</sup>

$$a_{ij}(s) = a_{ij} \left[ 1 + r_{ij} \frac{(s - s_{th})}{4m_{\pi^+}^2} \right] \tag{4.3}$$

where  $a_{ij}(s)$  are the ones defined in (4.1) but with  $a_0(s)$  and  $a_2(s)$ . For numerical applications, we use  $r_0 = 1.25 \pm 0.04$  and  $r_2 = 1.81 \pm 0.05$  [20] which are compatible with the results in [21] and

$$a_{+-}^P = a_{+0}^P = a_1/2 \tag{4.4}$$

with  $a_1^{CHPT} = m_\pi^2/(12\pi F_0^2)$  to lowest order in CHPT. The rest of  $a_{ij}^P$  are zero.

The above discussion fixes the real part of  $\pi\pi$  amplitudes to be used near threshold. Whenever  $\pi\pi$  amplitudes are evaluated very far from threshold (say  $s \sim m_K^2$ ) we use the real part of the full NLO CHPT expressions.

For the other ingredient needed in the optical theorem or in Cutkosky rules, i.e. the real part of  $K \rightarrow 3\pi$  amplitudes, the procedure we propose, in order to take into account

---

<sup>3</sup>The effects of  $\pi\pi$  threshold singularities are NNLO in a chiral counting and expected to be small. However one should include them since as we said we want to treat the  $\pi\pi$  scattering non-perturbatively – this can be done as in [16].

the re-scattering effects in a systematically improvable manner, is to treat it perturbatively within CHPT, i.e., first at tree-level (LO), next at one-loop (NLO),  $\dots$ . This is the main point of this analysis and the difference with the approach in [16]. It is the first step to go to NNLO and reduce the theoretical uncertainty to the percent level.

Notice that the use of the CHPT formula for the real part of  $K \rightarrow 3\pi$  does not change the need of fitting it to data. The aim is *not* to predict the real part of  $K \rightarrow 3\pi$  but to describe its analytic structure as accurately as possible so that, once separated the real part of  $K \rightarrow 3\pi$  from  $\pi\pi$  scattering through the optical theorem and Cutkosky rules, one can measure  $\pi\pi$  scattering near threshold as Cabibbo proposed. In particular,  $\pi\pi$  scattering near threshold is treated non-perturbatively as proposed in [14]. The advantage now is that we have the correct structure of singularities at a given CHPT order for real part of  $K \rightarrow 3\pi$  and this can be improved systematically. Below we give the formulas which describe the cusp effect at NLO within this approach.

#### 4.1 Cabibbo's Proposal for Charged Kaon Decays

Near  $\pi^+\pi^-$  threshold, we can decompose the  $K^+ \rightarrow \pi^0\pi^0\pi^+$  amplitude in the following way [14, 16]

$$A_{00+} = \begin{cases} \bar{A}_{00+} + \bar{B}_{00+}v_{\pm}(s_3), & s_3 > 4m_{\pi^+}^2, \\ \bar{A}_{00+} + i\bar{B}_{00+}v_{\pm}(s_3), & s_3 < 4m_{\pi^+}^2, \end{cases} \quad (4.5)$$

where  $\bar{A}_{00+}$  and  $\bar{B}_{00+}$  are in general singular functions except near the  $\pi^+\pi^-$  threshold [22] and

$$v_{ij}(s) = \sqrt{\frac{|s - (m_{\pi^{(i)}} + m_{\pi^{(j)}})^2|}{s}}. \quad (4.6)$$

Notice that these kinematical factors are taken with physical pion masses, in this way one can describe the cusp effect which is generated by the different behavior of  $K^+ \rightarrow \pi^0\pi^0\pi^+$  for the two neutral pions invariant energy above and below the  $s_3 = 4m_{\pi^+}^2$  threshold.

With these definitions, the differential decay rate for this amplitude can be written as [16]

$$|A_{00+}|^2 \equiv \text{Re}\bar{A}_{00+}^2 + \Delta_A + v_{\pm}(s_3)\Delta_{\text{cusp}}, \quad (4.7)$$

with

$$\Delta_A \equiv \text{Im}\bar{A}_{00+}^2 + v_{\pm}^2(s_3) \left[ \text{Re}\bar{B}_{00+}^2 + \text{Im}\bar{B}_{00+}^2 \right], \quad (4.8)$$

$$\Delta_{\text{cusp}} \equiv \begin{cases} -2\text{Re}\bar{A}_{00+}\text{Im}\bar{B}_{00+} + 2\text{Im}\bar{A}_{00+}\text{Re}\bar{B}_{00+}, & s_3 < 4m_{\pi^+}^2 \\ 2\text{Re}\bar{A}_{00+}\text{Re}\bar{B}_{00+} + 2\text{Im}\bar{A}_{00+}\text{Im}\bar{B}_{00+}, & s_3 > 4m_{\pi^+}^2. \end{cases} \quad (4.9)$$

The combination of real and imaginary amplitudes  $\Delta_{\text{cusp}}$  defined above parametrizes the cusp effect due to the  $\pi^+\pi^- \rightarrow \pi^0\pi^0$  re-scattering in the  $K^+ \rightarrow \pi^0\pi^0\pi^+$  decay rate, taking different values above and below the threshold  $s_3 = 4m_{\pi^+}^2$  associated to this re-scattering.

At this level, we can use the real part of the result for  $A_{00+}$  at one-loop in CHPT to fit data. We use it in the following. This provides a fit at least as good as the second order

polynomial parametrization used in the original proposal [14, 16] and its precision is just limited by data and the singularity structure at NLO in CHPT.

We get  $\text{Im}\overline{A}_{00+}$  and  $\text{Im}\overline{B}_{00+}$  using the optical theorem, where we consistently use the NLO expression for  $\text{Re } A_{00+}$  fitted to data.

The singular part of the dispersive amplitude, i.e.  $\text{Re}\overline{B}_{00+}v_{\pm}(s_3)$ , is proportional near threshold to one half of the discontinuity across the physical cut<sup>4</sup> which is also fixed just by unitarity and analyticity. We get the imaginary part of this discontinuity using the optical theorem while the real part is obtained applying Cutkosky rules. Some pieces of  $\text{Re}\overline{B}_{00+}$  can also be obtained going below  $\pi^+\pi^-$  threshold and applying the optical theorem there but one cannot get all of them in such way.

Notice that the accuracy with which we predict the cusp can be improved systematically by going at higher order in the loop expansion, which produces a more accurate singularity structure. The real part of the amplitude  $K^+ \rightarrow \pi^0\pi^0\pi^+$ , i.e.  $\text{Re } \overline{A}_{00+}$ , was calculated at NLO in CHPT in the isospin limit in [5, 9]. While the two-pion cut contributions to its dispersive part were calculated analytically at two-loops in [5] as explained in Section 3. The rest of the NLO contributions to the dispersive part of  $A_{00+}$  correspond to the three-pion cuts in topologies B, C and D in Figure 1 which are expected to be very small. They have been calculated here numerically for completeness and checked that they are negligible (see Appendix C for the results). They can be safely disregarded and we do not include them in our cusp effect formulas.

With those results at hand, we can study the scattering lengths combination  $a_0 - a_2$  determination from (4.9) using the NLO CHPT formulas for the real part of the  $K^+ \rightarrow \pi^0\pi^0\pi^+$  vertex in the optical theorem as explained above. For the real part of  $\pi^+\pi^- \rightarrow \pi^0\pi^0$  scattering we use the non-perturbative definition explained in Section 4. First, we give the expressions for the functions  $\overline{A}_{00+}$  and  $\overline{B}_{00+}$  using the tree-level CHPT expression to fit the real part of  $K^+ \rightarrow \pi^+\pi^0\pi^0$  to data, we get

$$\begin{aligned} \text{Re}\overline{A}_{00+}|_{LO}(s_1, s_2, s_3) &= C' \left[ \text{Re } G_8(m_\pi^2 - s_3) + G_{27} \frac{1}{16(m_K^2 - m_\pi^2)} \left[ s_3(4m_\pi^2 - 19m_K^2) + \right. \right. \\ &\quad \left. \left. + 5m_K^4 - 4m_\pi^4 + 19m_K^2m_\pi^2 \right] \right], \\ \text{Im}\overline{A}_{00+}|_{LO}(s_1, s_2, s_3) &= C' \left[ -v_{00}(s_3)a_{00}(s_3) \left[ \text{Re } G_8(s_3 - m_\pi^2) + G_{27} \frac{1}{6(m_K^2 - m_\pi^2)} \times \right. \right. \\ &\quad \times (4m_\pi^4 - 5m_K^4 - 19m_\pi^2m_K^2 - s_3(4m_\pi^2 - 19m_K^2)) \left. \right] + \\ &\quad + \left[ v_{+0}(s_1)(SW_{+0}^{LO}(s_1) + (s_2 - s_3)PW_{+0}^{LO}(s_1)) + s_1 \leftrightarrow s_2 \right], \\ SW_{+0}^{LO}(s) &= \frac{(s - 2m_\pi^2)}{64\pi f_\pi^2} \left[ \text{Re } G_8(m_K^2 + m_\pi^2 - s) + \frac{G_{27}}{6(m_K^2 - m_\pi^2)} (9m_K^4 + \right. \\ &\quad \left. + m_K^2(15m_\pi^2 - 19s) + 4m_\pi^2(s - m_\pi^2)) \right], \\ PW_{+0}^{LO}(s) &= \frac{(s - 4m_\pi^2)}{192\pi f_\pi^2} \left[ \text{Re } G_8 + \frac{G_{27}}{6(m_K^2 - m_\pi^2)} (19m_K^2 - 4m_\pi^2) \right], \end{aligned}$$

---

<sup>4</sup>We thank Jürg Gasser for clarifying this point to us.

$$\begin{aligned} \text{Re}\overline{B}_{00+}|_{LO}(s_3) &= 0, \\ \text{Im}\overline{B}_{00+}|_{LO}(s_3) &= C' a_x(s_3) \left[ -\text{Re} G_8(s_3 - m_\pi^2 + m_K^2) + G_{27} \frac{1}{3} [13s_3 - 7m_K^2 - 13m_\pi^2] \right], \end{aligned} \quad (4.10)$$

where  $C' = iC F_0^4/(f_\pi^3 f_K)$  and the constant  $C$  is defined in (2.3). Notice that  $LO$  here does not mean a calculation at LO fully in CHPT. It means that we have consistently used the LO CHPT expression to fit  $\text{Re}\overline{A}_{00+}$ , while  $\text{Im}\overline{B}_{00+}$ ,  $\text{Im}\overline{B}_{00+}$  which are obtained using the optical theorem start at  $\mathcal{O}(p^4)$  and  $\text{Re}\overline{B}_{00+}$  starts at  $\mathcal{O}(p^6)$ . In these expressions, we are always treating the  $\pi\pi$  scattering lengths to all orders.

Using the CHPT expression up to one-loop [5, 9] to fit the real part of  $K^+ \rightarrow \pi^0 \pi^0 \pi^+$  to data, we get near  $s_3 = 4m_{\pi^+}^2$  threshold

$$\begin{aligned} \text{Re}\overline{A}_{00+}|_{NLO}(s_1, s_2, s_3) &= \text{Re}\overline{A}_{00+}|_{LO} + \left[ M_7(s_3) + M_8(s_1) + M_8(s_2) + M_9(s_1)(s_2 - s_3) + \right. \\ &\quad \left. + M_9(s_2)(s_1 - s_3) \right]_{\mathcal{O}(p^4)} + \delta \text{Re}\overline{A}_{00+}(s_1, s_2, s_3), \\ \text{Im}\overline{A}_{00+}|_{NLO}(s_1, s_2, s_3) &= \text{Im}\overline{A}_{00+}|_{LO} + v_{00}(s_3) a_{00}(s_3) \left[ M_7(s_3) + \widetilde{M}_8(s_3) + \right. \\ &\quad \left. + \widetilde{M}_9(s_3)(m_K^2 + 3m_\pi^2 - 2s_3) - \widetilde{M}_9^s(s_3) \right]_{\mathcal{O}(p^4)} + \\ &\quad + \left[ v_{+0}(s_1)(SW_{+0}^{NLO}(s_1) + (s_2 - s_3)PW_{+0}^{NLO}(s_1)) + s_1 \leftrightarrow s_2 \right], \\ \text{Re}\overline{B}_{00+}|_{NLO}(s_3) &= -a_{00}(s_3) v_{00}(s_3) \text{Im}\overline{B}_{00+}(s_3) - \\ &\quad - a_x(s_3)^2 v_{00}(s_3) \int_{-1}^1 dx \text{Re}\overline{A}_{00+}(t^+(s_3, x), t^-(s_3, x), s_3) - \\ &\quad - a_x(s_3) \frac{1}{2} \int_{-1}^1 dx \text{Im}\widetilde{A}_{++-}(t^+(s_3, x), t^-(s_3, x)), \\ \text{Im}\overline{B}_{00+}|_{NLO}(s_3) &= \text{Im}\overline{B}_{00+}|_{LO} + a_x(s_3) \left[ 2M_{11}(s_3) + \widetilde{M}_{10}(s_3) + \widetilde{M}_{11}(s_3) - \right. \\ &\quad \left. - \widetilde{M}_{12}(s_3)(m_K^2 + 3m_\pi^2 - 2s_3) + \widetilde{M}_{12}^s(s_3) \right]_{\mathcal{O}(p^4)}, \end{aligned} \quad (4.11)$$

where we have neglected the three-pion cut graph contributions as explained above. And  $t^\pm(s, x) = a(s) \pm b(s)x$  with  $a(s)$  and  $b(s)$  defined in (B.2). The integration contour  $-1 \leq x \leq 1$  in  $\text{Re}\overline{B}_{00+}(s_3)$  is correct just for small values of  $s_3$  [23]<sup>5</sup>, namely,

$$4m_{\pi^0}^2 \leq s_3 \leq \frac{m_{\pi^0}}{m_{\pi^0} + m_{\pi^+}} (m_{K^+}^2 - m_{\pi^+}^2) \quad (4.12)$$

while for larger values of  $s_3$  there is an additional piece that takes into account the singularity at the pseudo-threshold  $s_3 = (m_{K^+} - m_{\pi^+})^2$  [23]. This piece can be calculated using a circuit in the complex- $x$  plane around a branch point and diverges at  $s_3 = (m_{K^+} - m_{\pi^+})^2$ .

The function  $\text{Im}\widetilde{A}_{++-}(t_1, t_2)$  we get from the imaginary part of the  $K^+ \rightarrow \pi^+ \pi^+ \pi^-$  decay amplitude defined in (2.1), which was obtained at order  $p^6$  in [5] using the optical theorem. From that result and disregarding the tiny contribution from the P wave, we get

$$\text{Im}\widetilde{A}_{++-}(t_1, t_2) = a_x(t_1) v_{00}(t_1) \int_{-1}^1 dy \text{Re}\overline{A}_{00+}(t^+(t_1, y), t^-(t_1, y), t_1) +$$

<sup>5</sup>We thank Jürg Gasser for bringing this work to our attention.

$$\begin{aligned}
& + 2a_{+-}(t_1)v_{\pm}(t_1) \int_{-1}^1 dy \operatorname{Re} \bar{A}_{++-}(t^+(t_1, y), t_1, t^-(t_1, y)) + \\
& + a_{++}(t_2)v_{\pm}(t_2) \int_{-1}^1 dy \operatorname{Re} \bar{A}_{++-}(t^+(t_2, y), t^-(t_2, y), t_2), \quad (4.13)
\end{aligned}$$

where the expression for  $\operatorname{Re} \bar{A}_{++-}$  at NLO in CHPT can be found in [5, 9]. This expression has to be fitted to  $K^+ \rightarrow \pi^+ \pi^+ \pi^-$  data. Notice that, in the formula above,  $\pi\pi$  amplitudes are sometimes evaluated very far from threshold. As said before, whenever this happens we use full NLO CHPT expressions and not only the scattering length approximation.

The contribution  $\delta \operatorname{Re} \bar{A}_{00+}$  comes from the discontinuity across the physical cuts and takes into account the singularities of  $\operatorname{Re} \bar{A}_{00+}$  at  $s_i = (m_{\pi^+} + m_{\pi^0})^2$  ( $i = 1, 2$ ) and  $s_3 = 4m_{\pi^0}^2$  thresholds which start at order  $p^6$  in CHPT. We get

$$\begin{aligned}
\delta \operatorname{Re} \bar{A}_{00+}(s_1, s_2, s_3) = & -a_{00}(s_3)v_{00}(s_3) \int_{-1}^1 dx \ a_{0+}(t^+(s_3, x))v_{0+}(t^+(s_3, x)) \times \\
& \times \int_{-1}^1 dy \operatorname{Re} \bar{A}_{00+}(t^+(s_3, x), t^+(t^+(s_3, x), y), t^-(t^+(s_3, x), y)) - \\
& - \left\{ a_{+0}(s_1)v_{+0}(s_1) \int_{-1}^1 dx \left[ \operatorname{Im} \bar{A}_{00+}(s_1, t^+(s_1, x), t^-(s_1, x)) + \right. \right. \\
& \left. \left. + v_{\pm}(t^-(s_1, x)) \operatorname{Im} \bar{B}_{00+}(t^-(s_1, x)) \right] + s_1 \rightarrow s_2 \right\}. \quad (4.14)
\end{aligned}$$

The integration contour  $-1 \leq x \leq 1$  in  $\delta \operatorname{Re} \bar{A}_{00+}(s_1, s_2, s_3)$  is correct just for  $s_3$  in the range (4.12) and for both  $s_1$  and  $s_2$  small, namely,

$$(m_{\pi^0} + m_{\pi^+})^2 \leq s_{1,2} \leq \frac{1}{2} (m_{K^+}^2 - m_{\pi^+}(2m_{\pi^0} - m_{\pi^+})). \quad (4.15)$$

For larger values of  $s_i$  the same comment after (4.12) applies, i.e., an additional piece which diverges as  $s_i$  approaches  $(m_{K^+} - m_{\pi^{(i)}})^2$  has to be added [23]. The problem arises here since we need to describe the discontinuity at the boundaries of the Dalitz plot for  $s_1$  (or for  $s_2$ ) when  $s_3$  is around threshold so that it is possible to approach the pseudo-thresholds in  $s_1$  (or in  $s_2$ ). One could think in putting a cut-off when integrating over  $s_1$  (and  $s_2$ ) such that one is far enough of the Dalitz boundary from below and still be able to see the cusp effect. We do not go further on this possibility in this paper. A solution to this problem which does not simply use the discontinuity to describe the cusp effect is discussed in [22].

In [16], they used the approximation that the integrands in (4.11), (4.13) and (4.14) are to a good accuracy linear in the variables  $x$  and  $y$ . If we make such approximation for the sake of comparison, we get

$$\begin{aligned}
\operatorname{Re} \bar{B}_{00+}|_{NLO}(s_3) = & -a_{00}(s_3)v_{00}(s_3) \operatorname{Im} \bar{B}_{00+}(s_3) - \quad (4.16) \\
& - 2a_x(s_3)^2 v_{00}(s_3) \operatorname{Re} \bar{A}_{00+}(a(s_3), a(s_3), s_3) - \\
& - 2a_x(s_3)a_x(a(s_3))v_{00}(a(s_3)) \operatorname{Re} \bar{A}_{00+}(a(a(s_3)), a(a(s_3)), a(s_3)) - \\
& - 4a_x(s_3)a_{+-}(a(s_3))v_{\pm}(a(s_3)) \operatorname{Re} \bar{A}_{++-}(a(a(s_3)), a(s_3), a(a(s_3))) - \\
& - 2a_x(s_3)a_{++}(a(s_3))v_{\pm}(a(s_3)) \operatorname{Re} \bar{A}_{++-}(a(a(s_3)), a(a(s_3)), a(s_3))
\end{aligned}$$

and

$$\begin{aligned}
\delta \text{Re} \overline{A}_{00+}(s_1, s_2, s_3) = & -4 a_{00}(s_3) a_{0+}(a(s_3)) v_{00}(s_3) v_{0+}(a(s_3)) \times \\
& \times \text{Re} \overline{A}_{00+}(a(s_3), a(a(s_3)), a(a(s_3))) - \\
& -2 \{ a_{+0}(s_1) v_{+0}(s_1) [\text{Im} \overline{A}_{00+}(s_1, a(s_1), a(s_1)) + \\
& + v_{\pm}(a(s_1)) \text{Im} \overline{B}_{00+}(a(s_1))] + s_1 \rightarrow s_2 \}
\end{aligned} \tag{4.17}$$

which agree with [16].

Again, in (4.11), the subscript  $NLO$  does not mean a calculation at NLO fully in CHPT. It means that we have consistently used the NLO CHPT isospin limit expression to fit  $\text{Re} \overline{A}_{00+}$  while the  $\pi\pi$  scattering lengths are treated to all orders. The chiral counting is applied just to the  $K^+ \rightarrow \pi^0 \pi^0 \pi^+$  vertex.

The contributions  $SW_{+0}^{NLO}(s_1)$  and  $PW_{+0}^{NLO}(s_1)$  were already calculated in [5] (the substitution  $\sigma(s_i) \rightarrow v_{+0}(s_i)$  in the formulas of [5] is understood) ,

$$\begin{aligned}
v_{+0}(s_1) SW_{+0}^{NLO}(s_1) + s_1 \leftrightarrow s_2 &= \text{formulas E.25 + E.29 of [5]} , \\
v_{+0}(s_1)(s_2 - s_3) PW_{+0}^{NLO}(s_1) + s_1 \leftrightarrow s_2 &= \text{formulas E.26 + E.30 of [5]} .
\end{aligned} \tag{4.18}$$

The functions  $M_i(s)$  used in (4.11) are the same functions defined in [9] at order  $p^4$  but exchanging the functions  $B(m_\pi, m_\pi, s_3)$  there by

$$\mathcal{B}(m_\pi, m_\pi, s_3) = \mathcal{J}(m_\pi, s_3) - \frac{1}{16\pi^2} \left[ \log \left( \frac{m_\pi^2}{\nu^2} \right) + 1 \right] \tag{4.19}$$

with

$$\mathcal{J}(m_\pi, s_3) = \frac{1}{16\pi^2} \begin{cases} 2 + v(s_3) \log \left( \frac{1-v(s_3)}{1+v(s_3)} \right) & s_3 > 4m_{\pi^+}^2 \\ 2 + 2v(s_3) \arctan(v(s_3)) & s_3 < 4m_{\pi^+}^2 \end{cases}$$

and  $v = \sqrt{|s - 4m_\pi^2|/s}$ . While  $\widetilde{M}_i$  and  $\widetilde{M}_i^s$  are defined in (B.1), in terms of the real part of the original  $M_i$  functions in [9].

The relative effect of the cusp in  $|A_{00+}|^2$  can be seen in Figure 2, where we plot  $\frac{d|\Gamma_{\text{cusp}}(s_3)|}{ds_3}$  over  $\frac{d\Gamma(s_3)}{ds_3}$  using the results in (4.11). Here,  $\Gamma_{\text{cusp}}$  is the contribution of  $v_{\pm}(s_3) \Delta_{\text{cusp}}(s_1, s_3)$  in (4.9) to the total  $K^+ \rightarrow \pi^0 \pi^0 \pi^+$  decay rate  $\Gamma$ ,

$$\frac{d\Gamma_{\text{cusp}}(s_3)}{ds_3} = \frac{1}{N} \int_{s_{1\min}}^{s_{1\max}} ds_1 v_{\pm}(s_3) \Delta_{\text{cusp}}(s_1, s_3) , \tag{4.20}$$

where  $N = 512\pi^3 m_K^3$ , and  $s_{1\max}$  and  $s_{1\min}$  can be found in Eq. (4.4) of [5]. In the integral above, we do not include the pieces that arise from the singularity at  $s_i = (m_{K^+}^2 - m_{\pi^{(i)}}^2)^2$  which makes  $\Delta_{\text{cusp}}(s_1, s_3)$  divergent as  $s_1$  approaches  $(m_{K^+}^2 - m_{\pi^0})^2$ . As commented above one could think in defining an observable by cutting-off  $s_1$  (and  $s_2$ ) and still be around threshold for  $s_3$ . For the sake of comparison with the results in [16] we just do not include those additional pieces in the rest of the numerics and leave for a future study such possibility.

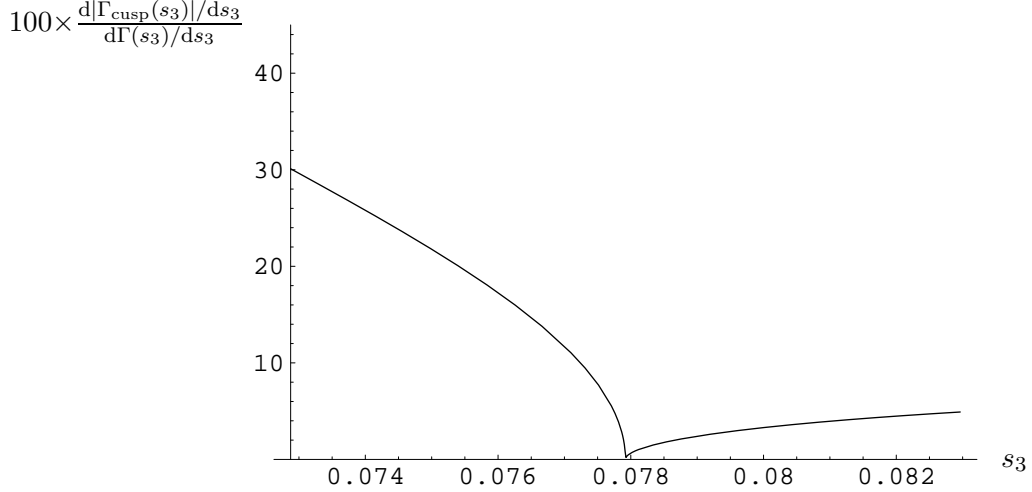


**Figure 2:** Plot of  $100 \times \frac{d|\Gamma_{\text{cusp}}(s_3)|/ds_3}{d\Gamma(s_3)/ds_3}$  around threshold as a function of  $s_3$ ,  $4m_{\pi^0}^2 \leq s_3 \leq 4(2m_{\pi^+}^2 - m_{\pi^0}^2)$ , for the decay  $K^+ \rightarrow \pi^0 \pi^0 \pi^+$ .

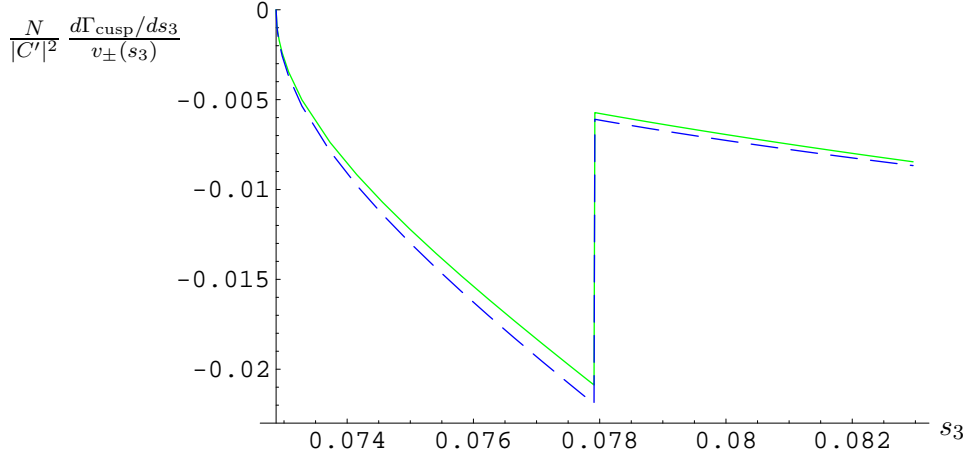


**Figure 3:** Plot of  $\frac{N}{|C'|^2} \frac{d\Gamma_{\text{cusp}}/ds_3}{v_{\pm}(s_3)}$  around threshold as a function of  $s_3$ ,  $4m_{\pi^0}^2 \leq s_3 \leq 4(2m_{\pi^+}^2 - m_{\pi^0}^2)$ , for the decay  $K^+ \rightarrow \pi^0 \pi^0 \pi^+$ . The meaning of the various lines is explained in the text.

In Figure 3, we show the cusp effect for  $K^+ \rightarrow \pi^0 \pi^0 \pi^+$  at NLO. The solid line is our result for  $\frac{N}{|C'|^2} \frac{d\Gamma_{\text{cusp}}/ds_3}{v_{\pm}(s_3)}$  in (4.9) using (4.11). The  $\pi\pi$  scattering lengths are unknowns to be fixed by fitting the cusp effect, however for the numerical comparison we take them as inputs given by CHPT [20] at NLO. For the rest of inputs needed for  $\text{Re}A_{00+}$  and  $\text{Re}\bar{A}_{+-}$  we use the ones in Appendix A, which have been obtained from a fit to data.

Using the same value of the  $\pi\pi$  scattering lengths, we also plot in Figure 3  $\frac{N}{|C'|^2} \frac{d\Gamma_{\text{cusp}}/ds_3}{v_{\pm}(s_3)}$  as obtained using the results in [16] –this is the dashed curve. For the slopes needed for  $\text{Re}A_{00+}$  and  $\text{Re}\bar{A}_{+-}$  in (4.6) and (4.7) in [16], we use the Taylor expansion of our results for  $\text{Re}A_{00+}$  and  $\text{Re}A_{+-}$ . This makes the comparison with the solid curve clearer. The effect of using instead the slopes from Taylor expanding  $|\text{Re}A_{00+}|^2 + |\text{Im}A_{00+}|^2$  and  $|\text{Re}A_{+-}|^2 + |\text{Im}A_{+-}|^2$ , respectively, amounts to increase the difference between solid and dashed curves by 2.5 % below threshold and 1 % above threshold.

If one compares the dashed curve and the solid one, one gets differences below threshold that vary between 7 % and 5 % while above threshold vary between 6 % and 2 %. The piece  $\text{Im}\bar{A}_{00+} \text{Re}\bar{B}_{00+}$ , which we include in the numerics and it was not in [16], is nominally order  $a^3$  and contributes to these differences by less than 1 %. This provides a first handle on the theoretical uncertainty of the Cabibbo's approach to obtain the scattering lengths since the differences between our approach and the one in [16] do not affect the treatment of  $\pi\pi$  scattering. The numerical differences we have described above are just due to the analytic form of  $\text{Re}\bar{A}_{00+}$  and to a lesser extent  $\text{Re}\bar{A}_{++-}$  –either a quadratic polynomial in  $s_3$  in [16] or the NLO in CHPT result here.

There are other sources of theoretical uncertainties; like for instance, the fit of the formulas to experimental data. In case of using CHPT NLO formulas for  $\text{Re}\bar{A}_{00+}$ , this fit produces central values of  $A_{00+}$  which agree with experiment within 3% accuracy [5, 9]. This global fit was done using total decay rates and Dalitz variable slopes. If one just used the data around threshold to make the fit, the accuracy would probably be at the 1% level or better. This uncertainty just measures how good is the fit of NLO CHPT formulas to experimental data.

A source of uncertainty which is more difficult to estimate and that is present in any approach which describes the cusp effect to NLO is the NNLO corrections. The only definite way to know it is to calculate them. In our approach, this means to calculate the real part of  $K^+ \rightarrow \pi^0\pi^0\pi^+$  at two-loop in the isospin conserving limit and make the same analysis that we have done but at NNLO. Notice that in this analysis the two-pion phase space factors are the physical ones in order to describe the cusp effect.

Meanwhile, we can just make the following estimate. Going from one order to the next one in our approach implies that new topologies with an extra  $\pi\pi$  scattering vertex are needed. For instance, topology B in Figure 1 appears when going from LO to NLO, and analogously there appear new topologies when going from NLO to NNLO. Following this line, a naive estimate of NNLO re-scattering effects in  $K \rightarrow 3\pi$  coincides numerically with the one made in [16], i.e., they would be suppressed by  $a_i^2$  with respect to LO. In fact one can expect the same typical 5 % theoretical uncertainty which is intrinsic of any NLO approximation of the cusp effect. As said above, it is possible to check this naive estimate by doing a two-loop calculation of the real part of  $K \rightarrow 3\pi$  in the isospin limit and going one order further in our approach.

A further source of error in the final determination of the scattering length  $a_0 - a_2$  from a fit to the cusp effect below threshold is due, as already discussed in [16], to the existence of different strategies to do the fit. The three basic ones are:

- One can consider all the  $a_i$  as free parameters in (4.11).
- All  $a_i$  are fixed to their standard values except the combination  $a_0 - a_2$  in  $a_x$  that is extracted from the fit.
- One can use CHPT as much as possible. Since the combination  $a_0 - a_2$ , or equivalently  $a_x(s_3)$ , only appears in  $\bar{B}_{00+}$ , which is proportional to the cusp, it is enough to keep

$\overline{B}_{00+}$  in terms of the scattering lengths. So that, one could fully use the CHPT predictions at NLO in [5, 9] for  $\text{Im } \overline{A}_{00+}$ .

The comparison of the results for  $a_x$  obtained from these different fit strategies will provide us with another handle to estimate the accuracy of the method. This uncertainty will become clear once the fits that we propose are done with data and to be added to the previous ones.

We want now to summarize the uncertainties that we have discussed and give our estimate for the total theoretical uncertainty. First, the final error from fitting the data to  $\text{Re } \overline{A}_{00+}$  measures the accuracy of the formula used to do the fit. This has to be checked once the real fit is done but we believe that it is realistic to assume that this theoretical uncertainty is around 2 %. The accuracy of the data should be at the few per cent level.

If this theoretical uncertainty from the fit is added to the 5 % of canonical uncertainty assigned to NNLO we get a theoretical uncertainty for the scattering lengths from the cusp effect in  $K^+ \rightarrow \pi^0 \pi^0 \pi^+$  between somewhat larger than 5 % (if uncertainties are added quadratically) and 7 % (if added linearly), i.e., we essentially agree therefore with the uncertainty quoted by [16]. Notice that we get our final theoretical uncertainty as the sum (either linear or quadratic) of several order 1% to 2% uncertainties to the canonical NNLO 5 % uncertainty.

Yet, as noted before, we find numerical differences between our approach and the one in [16] of the same order as the 5 % of NNLO quoted error both below and above threshold. These numerical differences are just due to the different analytic form used for  $\text{Re } \overline{A}_{00+}$  and (to a much lesser extent) to the analytic form of  $\text{Re } \overline{A}_{++-}$ .

To the uncertainties discussed above, one still has to add the one from the different data fitting strategies described above.

## 4.2 Cabibbo's Proposal for Neutral Kaons

In the neutral kaon channel it is also possible to measure the scattering lengths combination  $a_0 - a_2$  from the cusp effect in the energy spectrum of two  $\pi^0$  of  $K_L \rightarrow \pi^0 \pi^0 \pi^0$ . In this case the Bose symmetry of the three neutral pions implies that the amplitude is completely symmetric for the interchanges  $s_1 \leftrightarrow s_2 \leftrightarrow s_3$ . The amplitude near  $\pi^+ \pi^-$  threshold can be written as [16]

$$A_{000} = \begin{cases} \sum_{i=1,2,3} \{ \overline{A}_{000}(s_i) + v_{\pm}(s_i) \overline{B}_{000}(s_i) \} , & \text{if all } s_i > 4m_{\pi^+}^2 ; \\ \sum_{i=1,2,3} \{ \overline{A}_{000}(s_i) \} + i v_{\pm}(s_k) \overline{B}_{000}(s_k) + \\ + \sum_{\substack{i=1,2,3 \\ i \neq k}} \{ v_{\pm}(s_i) \overline{B}_{000}(s_i) \} , & \begin{cases} s_k < 4m_{\pi^+}^2, \\ k = 1, 2, 3 \\ s_{i \neq k} > 4m_{\pi^+}^2 . \end{cases} \end{cases} \quad (4.21)$$

The crucial observation in (4.21) is that if the value of say  $s_k$  is below threshold, the other two variables  $s_i$  ( $i \neq k$ ) are of order  $(m_K^2 - m_{\pi^+}^2)/2$ , so safely above threshold. Thus it is kinematically impossible to cross the threshold with all three variables  $s_i$  at the same time.

Let us suppose now that we look at the region where the variable  $s_3$  is around threshold. In this region one can define,

$$\begin{aligned}\overline{A}'_{000}(s_1, s_2, s_3) &= \sum_{i=1,2,3} \overline{A}_{000}(s_i) + \sum_{i=1,2} v_{\pm}(s_i) \overline{B}_{000}(s_i) , \\ \overline{B}'_{000}(s_3) &= \overline{B}_{000}(s_3) .\end{aligned}\quad (4.22)$$

Equations (4.7)-(4.9) are now valid also for the decay of  $K_L \rightarrow \pi^0 \pi^0 \pi^0$  once the substitutions  $A_{00+} \rightarrow A_{000}$ ,  $\overline{A}_{00+} \rightarrow \overline{A}'_{000}$  and  $\overline{B}_{00+} \rightarrow \overline{B}'_{000}$  are done.

Again, we can write these amplitudes substituting the approximation (4.3) for the amplitudes near threshold. The amplitudes contain  $\pi\pi$  re-scattering in all channels and to treat them we use full CHPT expressions when they are very far from threshold, which as explained in Section 4 is a better approximation than using scattering lengths.

The absorptive and the singular part of the dispersive part are calculated analogously to the charged kaon case – see Section 4.1.

Using one-loop for the real part of  $K_L \rightarrow \pi^0 \pi^0 \pi^0$ , one then finds

$$\begin{aligned}\text{Re} \overline{A}'_{000}|_{LO}(s_1, s_2, s_3) &= C' (\text{Re} G_8 - G_{27}) m_K^2 , \\ \text{Im} \overline{A}'_{000}|_{LO}(s_1, s_2, s_3) &= C' \left[ v_{00}(s_3) a_{00}(s_3) + \frac{m_\pi^2}{32\pi f_\pi^2} (v_{00}(s_1) + v_{00}(s_2)) \right] m_K^2 (\text{Re} G_8 - G_{27}) + \\ &\quad + \frac{s_1 - m_\pi^2}{16\pi f_\pi^2} f_{000}(s_1) + \frac{s_2 - m_\pi^2}{16\pi f_\pi^2} f_{000}(s_2) , \\ \text{Re} \overline{B}'_{000}|_{LO}(s_3) &= 0 , \\ \text{Im} \overline{B}'_{000}|_{LO}(s_3) &= 2a_x(s_3) f_{000}(s_3) , \\ \text{with } f_{000}(s) &= C' \left[ \text{Re} G_8 (s - m_\pi^2) + \frac{G_{27}}{6(m_K^2 - m_\pi^2)} (s(9m_K^2 - 24m_\pi^2) - 5m_K^4) + \right. \\ &\quad \left. + 24m_\pi^2 + m_\pi^2 m_K^2) \right] .\end{aligned}\quad (4.23)$$

The meaning of  $LO$  here is the same that in (4.10).

The effect of the charged pion re-scattering appears also at NLO,

$$\begin{aligned}\text{Re} \overline{A}'_{000}|_{NLO}(s_1, s_2, s_3) &= \text{Re} \overline{A}'_{000}|_{LO} + \left[ M_0(s_1) + M_0(s_2) + M_0(s_3) \right]_{\mathcal{O}(p^4)} + \\ &\quad + \delta \text{Re} \overline{A}'_{000}(s_1, s_2, s_3) , \\ \text{Im} \overline{A}'_{000}|_{NLO}(s_1, s_2, s_3) &= \text{Im} \overline{A}'_{000}|_{LO} + v_{00}(s_3) a_{00}(s_3) \left[ M_0(s_3) + \widetilde{M}_0(s_3) \right]_{\mathcal{O}(p^4)} + \\ &\quad + \left[ \text{Im} A_W^{(6,1)}(s_1) + \text{Im} A_W^{(6,2)}(s_1) + \right. \\ &\quad \left. + \text{Im} A_\pi^{(6,1)}(s_1) + \text{Im} A_\pi^{(6,2)}(s_1) + s_1 \leftrightarrow s_2 \right] , \\ \text{Re} \overline{B}'_{000}|_{NLO}(s_3) &= F_{000}(s_3) , \\ \text{Im} \overline{B}'_{000}|_{NLO}(s_3) &= \text{Im} \overline{B}'_{000}|_{LO} + 2a_x(s_3) \left[ M_1(s_3) + \widetilde{M}_2(s_3) + \right. \\ &\quad \left. + \widetilde{M}_3(s_3)(m_K^2 + 3m_\pi^2 - 2s_3) - \widetilde{M}_3^s(s_3) \right]_{\mathcal{O}(p^4)} ,\end{aligned}\quad (4.24)$$

where we neglected the contributions of three-pion cut graphs which have been shown to be very small in Appendix C and the function  $F_{000}(s)$  has the expression

$$\begin{aligned} F_{000}(s) = & -a_{00}(s)v_{00}(s)\text{Im}\overline{B}_{000}(s) - \\ & -2a_x(s)^2v_{00}(s)\left\{\text{Re}\overline{A}_{000}(s) + \int_{-1}^1 dx \text{Re}\overline{A}_{000}(t^+(s, x))\right\} - \\ & -a_x(s)\int_{-1}^1 dx \text{Im}\tilde{A}_{+-0}^L(t^+(s, x), t^-(s, x)). \end{aligned} \quad (4.25)$$

Above, the integration contour  $-1 \leq x \leq 1$  in  $\text{Re}F_{000}(s)$  is correct just for small values of  $s$ , namely [23], for

$$4m_{\pi^0}^2 \leq s \leq \frac{1}{2}(m_{K^0}^2 - m_{\pi^0}^2). \quad (4.26)$$

For larger values of  $s$  there is an additional piece [23] and the same comments and discussion after (4.12) apply here.

The functions  $\text{Im}A_j^{(6,i)}(s)$  are given in Appendix B.2 and the meaning of  $NLO$  in (4.24) is the same that in (4.11). The imaginary part of the  $K_L \rightarrow \pi^+(p_1)\pi^-(p_2)\pi^0(p_3)$  decay amplitude,  $\text{Im}\tilde{A}_{+-0}^L(t_1, t_2, t_3)$ , has been obtained here at order  $p^6$  using the optical theorem. See Section 3 and Appendix B.3 for the full expression. From that result, disregarding the tiny contribution from the P wave and the pieces that do not contribute to singularities, the function  $\text{Im}\tilde{A}_{+-0}^L(t_1, t_2)$  is

$$\begin{aligned} \text{Im}\tilde{A}_{+-0}^L(t_1, t_2) = & a_{+0}(t_1)v_{+0}(t_1)\int_{-1}^1 dy \text{Re}\overline{A}_{+-0}^L(t_1, t^+(t_1, y), t^-(t_1, y)) \\ & + t_1 \rightarrow t_2, \end{aligned} \quad (4.27)$$

where the expression for  $\text{Re}\overline{A}_{+-0}^L$  at NLO in CHPT can be found in [5, 9]. This expression has to be fitted to  $K_L \rightarrow \pi^+\pi^-\pi^0$  data. Notice that, in the formula above,  $\pi\pi$  amplitudes are sometimes evaluated very far from threshold. As said before, whenever this happens we use full NLO CHPT expressions and not only the scattering length approximation.

The contribution  $\delta\text{Re}\overline{A}'_{000}$  comes from the discontinuity across the physical cuts and takes into account just the singularities of  $\text{Re}\overline{A}'_{000}$  at  $s_i = 4m_{\pi^+}^2$ ,  $s_i = (m_{\pi^+} + m_{\pi^0})^2$  and  $s_i = 4m_{\pi^0}^2$  ( $i = 1, 2$ ) thresholds which start at order  $p^6$  in CHPT. We get

$$\begin{aligned} \delta\text{Re}\overline{A}'_{000}(s_1, s_2, s_3) = & \sum_{i=1,2} v_{\pm}(s_i) F_{000}(s_i) - \sum_{i=1,2,3} v_{00}(s_i) a_{00}(s_i) \times \\ & \times \int_{-1}^1 dx \left\{ a_{00}(t^+(s_i, x))v_{00}(t^+(s_i, x)) \left[ \text{Re}\overline{A}_{000}(t^+(s_i, x)) + \right. \right. \\ & \left. \left. + \int_{-1}^1 dy \text{Re}\overline{A}_{000}(t^+(t^+(s_i, x), y)) \right] + a_x(t^+(s_i, x))v_{\pm}(t^+(s_i, x)) \times \right. \\ & \left. \times \int_{-1}^1 dy \text{Re}\overline{A}_{+-0}(t^+(t^+(s_i, x), y), t^-(t^+(s_i, x), y), t^+(s_i, x)) \right\}. \end{aligned} \quad (4.28)$$

Above, the integration contour  $-1 \leq x \leq 1$  is correct just for all  $s_3$ ,  $s_1$  and  $s_2$  small, namely, all in the range in (4.26). For larger values of  $s_i$ , the same discussion after (4.15) applies.

In [16], they used the approximation that the integrands in (4.24), (4.27) and (4.28) are to a good accuracy linear in the variables  $x$  and  $y$ . If we made such approximation for the sake of comparison, we get

$$\begin{aligned} \text{Re}\overline{B}'_{000}(s_3) = & -a_{00}(s_3)v_{00}(s_3)\text{Im}\overline{B}_{000}(s_3) - \\ & -2a_x(s_3)^2v_{00}(s_3)\left\{\text{Re}\overline{A}_{000}(s_3) + 2\text{Re}\overline{A}_{000}(a(s_3))\right\} - \\ & -8a_x(s_3)a_{+0}(a(s_3))v_{+0}(a(s_3))\text{Re}\overline{A}_{+-0}^L(a(s_3), a(a(s_3)), a(a(s_3))) \end{aligned} \quad (4.29)$$

and

$$\begin{aligned} \delta\text{Re}\overline{A}'_{000}(s_1, s_2, s_3) = & -\sum_{i=1,2}v_{\pm}(s_i)\left\{a_{00}(s_i)v_{00}(s_i)\text{Im}\overline{B}_{000}(s_i) + \right. \\ & +2a_x(s_i)^2v_{00}(s_i)\left[\text{Re}\overline{A}_{000}(s_i) + 2\text{Re}\overline{A}_{000}(a(s_i))\right] + \\ & +8a_x(s_i)a_{+0}(a(s_i))v_{+0}(a(s_i))\text{Re}\overline{A}_{+-0}^L(a(s_i), a(a(s_i)), a(a(s_i)))\left.\right\} - \\ & -2\sum_{i=1,2,3}a_{00}(s_i)v_{00}(s_i)\left\{a_{00}(a(s_i))v_{00}(a(s_i)) \times \right. \\ & \times\left[\text{Re}\overline{A}_{000}(s_i) + 2\text{Re}\overline{A}_{000}(a(s_i))\right] + \\ & \left.+2a_x(a(s_i))v_{\pm}(a(s_i))\text{Re}\overline{A}_{+-0}^L(a(a(s_i)), a(a(s_i)), a(s_i))\right\} \end{aligned} \quad (4.30)$$

which agree with [16] up to the terms proportional to  $v_{00}(a(s_i))$  and  $v_{\pm}(a(s_i))$  in  $\delta\text{Re}\overline{A}'_{000}$ , which were not included there.

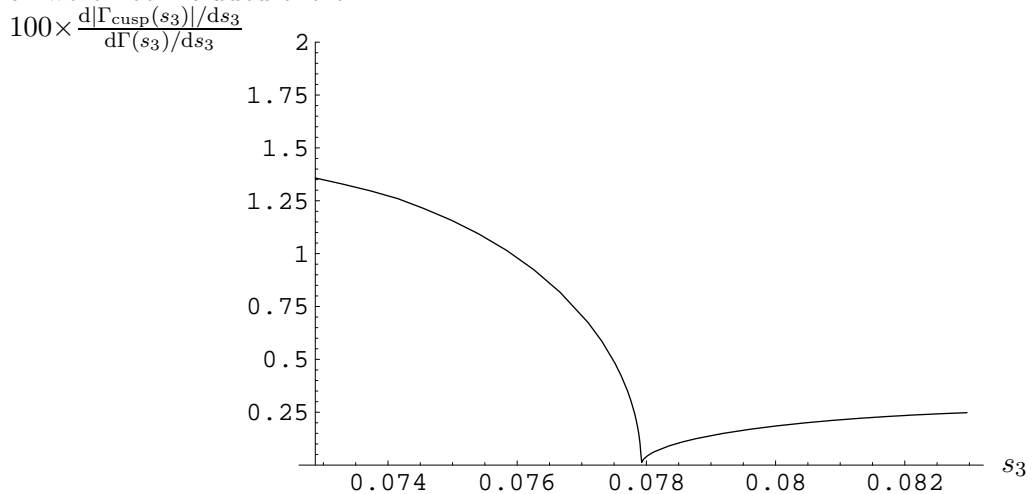


**Figure 4:** Plot of  $100 \times \frac{d|\Gamma_{\text{cusp}}(s_3)|}{ds_3}$  over  $\frac{d\Gamma(s_3)}{ds_3}$  around threshold as a function of  $s_3$ ,  $4m_{\pi^0}^2 \leq s_3 \leq 4(2m_{\pi^+}^2 - m_{\pi^0}^2)$ , for the decay  $K_L \rightarrow \pi^0\pi^0\pi^0$ .

In Figure 4 we show the ratio  $100 \times \frac{d|\Gamma_{\text{cusp}}(s_3)|}{ds_3}$  over  $\frac{d\Gamma(s_3)}{ds_3}$  using the results in (4.24) for  $K_L \rightarrow \pi^0\pi^0\pi^0$ . Here,  $\Gamma_{\text{cusp}}$  is the contribution of  $v_{\pm}(s_3)\Delta_{\text{cusp}}(s_1, s_3)$  in (4.9) to the total

$K_L \rightarrow \pi^0 \pi^0 \pi^0$  decay rate  $\Gamma$ . Above threshold the effect is extremely small and can hardly be distinguished.

In the integral over  $s_1$  in (4.20) define  $d|\Gamma_{\text{cusp}}(s_3)|/ds_3$  we do not include the additional pieces discussed after (4.26) for the sake of numerical comparison with the results in [16]. An analogous discussion to the one after (4.20) applies in this case as well.

In Figure 5 we plot the cusp effect  $\frac{3N}{|C'|^2} \frac{d\Gamma_{\text{cusp}}/ds_3}{v_{\pm}(s_3)}$  in (4.9) for  $K_L \rightarrow \pi^0 \pi^0 \pi^0$  at NLO. The solid line are our results in (4.24). For the numerical comparison we use the same inputs as for the charged case explained in the previous section.

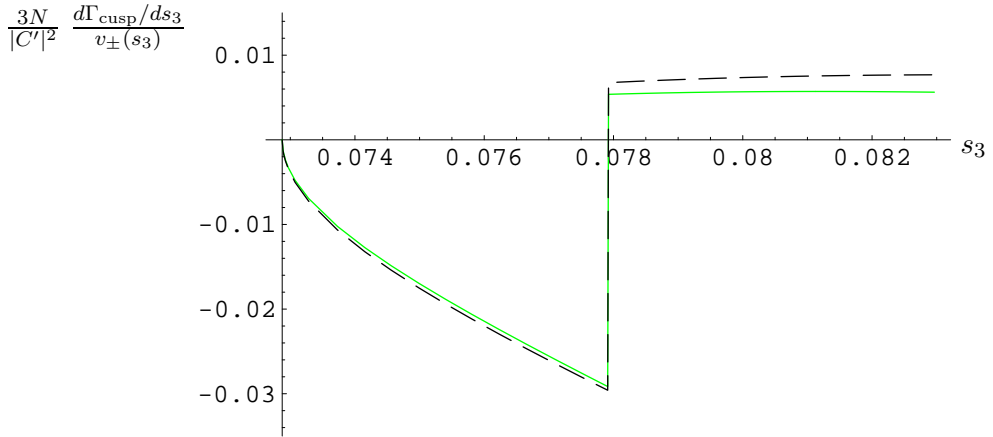


**Figure 5:** Plot of  $\frac{3N}{|C'|^2} \frac{d\Gamma_{\text{cusp}}/ds_3}{v_{\pm}(s_3)}$  around threshold as a function of  $s_3$ ,  $4m_{\pi^0}^2 \leq s_3 \leq 4(2m_{\pi^+}^2 - m_{\pi^0}^2)$  for the decay  $K_L \rightarrow \pi^0 \pi^0 \pi^0$ . The meaning of the various lines is explained in the text.

We also plot in Figure 3  $\frac{3N}{|C'|^2} \frac{d\Gamma_{\text{cusp}}/ds_3}{v_{\pm}(s_3)}$  using the results in [16] –this is the dashed curve. For the slopes needed for  $\text{Re}A_{000}^L$  and  $\text{Re}\bar{A}_{+-0}^L$  in (4.58) and (4.59) in [16], we use the Taylor expansion of our results for  $\text{Re}A_{000}^L$  and  $\text{Re}A_{+-0}^L$ . This makes the comparison with the solid curve clearer. The numerical differences between solid and dashed curves increase by around 2.5 % if instead we use the slopes from Taylor expanding  $|\text{Re}A_{000}^L|^2 + |\text{Im}A_{000}^L|^2$  and  $|\text{Re}A_{+-0}^L|^2 + |\text{Im}A_{+-0}^L|^2$ , respectively.

If one compares the dashed curve with the solid one below threshold, one gets differences between 6 % and 2 %. The part of the singularities in  $\delta\text{Re}\bar{A}_{000}$  that was not included in [16] –see comment after (4.30)– and that we do include in the solid line contributes in about + 2 % to this difference. The piece  $\text{Im}\bar{A}_{000}^L \text{Re}\bar{B}_{000}^L$ , which we include and it was not in [16], is nominally order  $a^3$  and contributes to these differences by less than 1 %.

Notice again that the differences between our approach and the one in [16] do not affect to the treatment of the  $\pi\pi$  scattering part. These numerical differences are just due to the different analytic form used for  $\text{Re}\bar{A}_{000}^L$  and to a lesser extent to the analytic form of  $\text{Re}\bar{A}_{+-0}^L$ .

Above threshold, there are large numerical cancellations between  $\text{Im}\bar{A}_{000}^L \text{Im}\bar{B}_{000}^L$  and  $\text{Re}\bar{A}_{000}^L \text{Re}\bar{B}_{000}^L$  in the corresponding expression for the cusp in  $K_L \rightarrow \pi^0 \pi^0 \pi^0$  (see (4.9) for the charged case). As a consequence, one should know both the real and imaginary parts of  $\bar{A}_{000}^L$  and  $\bar{B}_{000}^L$  better than at the 1 % level to predict the cusp above threshold with

an uncertainty around 5 %. This fact makes the region above threshold not suitable to extract the scattering lengths in  $K_L \rightarrow \pi^0 \pi^0 \pi^0$ .

As for the charged case, one has to add to the theoretical uncertainty the final error from the fitting to  $\text{Re} \bar{A}_{000}$  which includes the theoretical error which measures the accuracy of the formula used to do the fit. As said above, this has to be checked once the real fit is done but we believe that it is realistic to assume that this theoretical uncertainty is around 2 %. Again, the accuracy of the data should be at the level of a few per cent as for the charged case.

If this is added to the 5 % of canonical uncertainty assigned to NNLO we get a theoretical uncertainty for the scattering lengths combination  $a_0 - a_2$  from the cusp effect in  $K_L \rightarrow \pi^0 \pi^0 \pi^0$  between somewhat larger than 5 % (if uncertainties are added quadratically) and 7 % (if added linearly). I.e., we predict a similar theoretical accuracy in the extraction of  $a_0 - a_2$  from neutral and charged kaon cusp effects. But notice that in the neutral case, this uncertainty just applies to the analysis of the data below threshold. As said before, there are very large numerical cancellations above threshold which preclude the use of these data.

To the uncertainties discussed above, one still has to add the one from the different data fitting strategies as described in Section 4.1.

## 5. Summary and Conclusions

In Section 3, we have presented the full FSI phases for  $K \rightarrow 3\pi$  at NLO in CHPT, i.e. at  $\mathcal{O}(p^6)$  analytically. The two-pion cut contributions for  $K^+ \rightarrow 3\pi$  were already presented in [5]. We complete the calculation here with the three-pion cut contributions and the full result for  $K_{L,S} \rightarrow 3\pi$ . The two-pion cut contributions are given analytically while the three-pion cut ones are done numerically and checked always to be negligible. We used the techniques already explained in [5] which are based on perturbative unitarity and analyticity of CHPT.

In Section 4.1, we use these results to study Cabibbo's proposal to measure the scattering lengths combination  $a_0 - a_2$  from the cusp effect in the total  $\pi^0 \pi^0$  pair energy spectrum in  $K^+ \rightarrow \pi^0 \pi^0 \pi^+$  [14, 16]. We studied also the analogous proposal for  $K_L \rightarrow \pi^0 \pi^0 \pi^0$  in Section 4.2. Using the result found in Section 3 that the three-pion cut contributions are negligible –see also [16], we just include the two-pion cut contributions in the description of the cusp effect. We would like to remark here that making the same approximations that were done in [16] we agree fully with their analytical results.

The cusp effect originates in the different contributions to  $K^+ \rightarrow \pi^0 \pi^0 \pi^+$  and  $K_L \rightarrow \pi^0 \pi^0 \pi^0$  amplitudes above and below threshold of  $\pi^+ \pi^-$  production in the  $\pi^0 \pi^0$  pair invariant energy. We obtain these contributions using just analyticity and unitarity, in particular applying Cutkosky rules and the optical theorem above and below threshold to calculate the discontinuity across the physical cut. This allows us to separate the real part of  $K^+ \rightarrow \pi^0 \pi^0 \pi^+$  and  $K_L \rightarrow \pi^0 \pi^0 \pi^0$  contributions from the  $\pi\pi$  scattering which we want to measure. The real part of the discontinuity has a singularity when any of the  $s_i$  invariant energy reaches its pseudo-threshold at  $(m_K - m_{\pi^{(i)}})^2$  as described in [23]. We have

discussed how this singularity appears in our formulas for the discontinuity and discussed the problems that this poses for the description of the cusp effect using the discontinuity – see Section 4.1 and Section 4.2. One may think of using a upper cut-off in  $s_1$  (and  $s_2$ ) to define the cusp effect and compare with data, we however do not follow this possibility any further in this work and leave it for a possible future study. For a possible solution of this problem which does not simply use the discontinuity to describe the cusp effect see [22].

For the description of the cusp, we treat  $\pi\pi$  scattering lengths no-perturbatively as it was done in [16] but for the real part of  $K^+ \rightarrow \pi^0\pi^0\pi^+$  and  $K_L \rightarrow \pi^0\pi^0\pi^0$  we use the CHPT formulas at NLO. Notice that we do not use CHPT to predict the real part of  $K^+ \rightarrow \pi^0\pi^0\pi^+$ ,  $K_L \rightarrow \pi^0\pi^0\pi^0$ ,  $K^+ \rightarrow \pi^+\pi^+\pi^-$  and  $K_L \rightarrow \pi^+\pi^-\pi^0$ , but use their analytical form at NLO to fit it to data above threshold. In [16], the authors used a quadratic polynomial in  $s_3$  to make this fit to data. We choose to use the CHPT formulas at NLO which contain the correct analytical structure at that order and can be improved by going to the next order. We studied how much differ numerically these two different choices. The treatment of  $\pi\pi$  scattering is independent of these choices and we do it in the same way as in [16], i.e. non-perturbatively as said before.

We also discussed in Sections 4.1 and 4.2. the theoretical uncertainties we get for  $a_0 - a_2$  if one uses our formulas to fit the experimental data. We conclude that for  $K^+ \rightarrow \pi^0\pi^0\pi^+$ , this uncertainty is somewhat larger than 5 % if uncertainties are added quadratically and 7 % if added linearly, always in the isospin limit. I.e., we essentially agree with the estimate in [16]. Notice that we get our final theoretical uncertainty as the sum of several order 1% to 2% uncertainties to the canonical NNLO 5 % uncertainty.

Yet, as noted in Section 4.1 we find numerical differences for  $K^+ \rightarrow \pi^0\pi^0\pi^+$  between our approach and the one in [16] of the same order or larger than the NNLO 5% canonical error both above and below threshold. These numerical differences are just due to the different analytic form used for  $\text{Re}\bar{A}_{00+}$  and (to a much lesser extent) to the analytic form of  $\text{Re}\bar{A}_{+-+}$ .

For the case  $K_L \rightarrow \pi^0\pi^0\pi^0$ , we get that the uncertainty in the determination of  $a_0 - a_2$  is of the same order as for  $K^+ \rightarrow \pi^0\pi^0\pi^+$  if one uses the data below threshold and again in the isospin limit. Above threshold we found large numerical cancellations which preclude from using it to measure the scattering lengths combination  $a_0 - a_2$ .

In this case, the numerical differences we find between our approach and the one in [16] due to the different analytic form used for  $\text{Re}\bar{A}_{000}$  and (to a much lesser extent) to the analytic form of  $\text{Re}\bar{A}_{+-0}$  range between 6 % and 2 % below threshold, see Section 4.2. Which are again of the same order as the NNLO 5% canonical error.

Notice that, in addition to these uncertainties, there are numerical differences induced by using either a second order polynomial [16] or CHPT formulas at NLO, in both cases fitted to data, to describe the real part of  $K^+ \rightarrow \pi^0\pi^0\pi^+$ . These numerical differences are of the same order as the canonical NNLO 5 % error. The analogous differences for  $K_L \rightarrow \pi^0\pi^0\pi^0$  are very small. A reason in favor of using the CHPT form at NLO is that it includes the correct analytical structure up to NLO and one can improve this systematically by going to higher orders in CHPT.

An expansion in the scattering lengths  $a_i$  was used in [16] to obtain their NLO de-

scription of the cusp effect in  $K^+ \rightarrow \pi^0 \pi^0 \pi^+$  and uncertainty estimate and used Feynman diagrams to do the power counting. Notice that at each higher CHPT loop order there appear new topologies in  $K \rightarrow 3\pi$  which are of order  $a_i^{(n+1)}$  at the  $n$ -loop order. As a result one cannot expect to decrease the 5% theoretical uncertainty of the NLO result unless one computes the full NNLO isospin conserving  $K \rightarrow 3\pi$  amplitude. We conclude that if one wants to reach the percent level in the uncertainty of the determination of  $a_0 - a_2$  from the cusp effect, one would need to go to NNLO (two-loop in the dispersive part) in the re-scattering effects in the isospin limit. Recall also that a perturbative loop expansion like CHPT is not an expansion in powers of  $a_i$ .

Our CHPT approach can be improved order by order and a quantitative analysis at NNLO analogous to the one done here can provide a detailed estimate of the error at that level. We have just included isospin breaking due to the different thresholds using two-pion physical phase spaces in the optical theorem and Cutkosky rules. This is needed to describe the cusp effect. The rest of NLO isospin breaking is expected to be important just at NNLO order. At that order, the already calculated NLO  $K \rightarrow 3\pi$  isospin breaking corrections [12, 13] and isospin breaking effects in  $\pi\pi$  scattering at threshold at the same order will have to be implemented and their uncertainties added.

Finally, we believe that it is interesting to continue investigating the proposal in [14, 16] to measure the non-perturbative  $\pi\pi$  scattering lengths from the cusp effect in  $K^+ \rightarrow \pi^0 \pi^0 \pi^+$  and  $K_L \rightarrow \pi^0 \pi^0 \pi^0$ . In particular, to further reduce the theoretical uncertainties found here, a two-loop calculation in the isospin limit of those  $K \rightarrow 3\pi$  decays is needed. Another interesting direction is to develop an effective field theory in the scattering lengths which could both check the results in [16] and allow to go to NNLO. This type of studies is already underway and firsts results were presented [19, 22].

## Acknowledgments

It is a pleasure to acknowledge useful discussions with Hans Bijnens, Jürg Gasser, Gino Isidori and Toni Pich. This work has been supported in part by European Commission (EC) RTN Network EURIDICE Contract No. HPRN-CT2002-00311 (J.P. and I.S.), the Hadron-Physics I3 Project (EC) Contract No. RII3-CT-2004-506078 (E.G.), by MEC (Spain) and FEDER (EC) Grant Nos. FPA2003-09298-C02-01 (J.P.) and FPA2004-00996 (I.S.), and by Junta de Andalucía Grants No. FQM-101 (E.G. and J.P.) and FQM-347 (J.P.). E.G. is indebted to the EC for the Marie Curie Fellowship No. MEIF-CT-2003-501309. I.S. wants to thank the Departament d'ECM, Facultat de Física, Universitat de Barcelona (Spain) for kind hospitality.

## Appendices

### A. Numerical Inputs

Here we discuss the numerical inputs we use in the numerical applications. In [9], a fit to all available  $K \rightarrow \pi\pi$  amplitudes at NLO in CHPT and  $K \rightarrow 3\pi$  amplitudes and slopes

in  $K \rightarrow 3\pi$  amplitudes was done. All these was done in the isospin limit. More recently, this fit was updated in [13] with new data on slopes and including also the full isospin breaking effects. Though our calculation of FSI at NLO uses isospin limit results we will use the results obtained in this last fit. The reason is that the change in the fit results is due to both the new data used and the isospin breaking corrections at the same level and therefore cannot be disentangled. In addition, the main isospin breaking effects due to the kinematical factors is also taken into account in our results.

At lowest CHPT order  $p^2$ , the results in [13] are equivalent [using  $F_0 = 87.7$  MeV] to

$$\begin{aligned} \text{Re } G_8 &= 6.6 \pm 1.1 \quad \text{and} \\ G_{27} &= 0.44 \pm 0.09. \end{aligned} \quad (\text{A.1})$$

In this normalization,  $\text{Re } G_8 = 1 = G_{27}$  at large  $N_c$ . ( $N_c$  is the number of colors of QCD).

For the NLO prediction of the FSI, we only need the real part of the counterterms and in particular the combinations in Table 1 of [5] which from the new fit in [13] are given in Table 1. These were obtained from a fit of the NLO in CHPT results to experimental data.

	$\text{Re } \tilde{K}_i(M_\rho)$ from [13]
$\tilde{K}_2(M_\rho)$	$G_8 \times (48.5 \pm 2.4) \cdot 10^{-3}$
$\tilde{K}_3(M_\rho)$	$G_8 \times (2.6 \pm 1.2) \cdot 10^{-3}$
$\tilde{K}_5(M_\rho)$	$-G_{27} \times (41.2 \pm 16.9) \cdot 10^{-3}$
$\tilde{K}_6(M_\rho)$	$-G_{27} \times (102 \pm 105) \cdot 10^{-3}$
$\tilde{K}_7(M_\rho)$	$G_{27} \times (78.6 \pm 33) \cdot 10^{-3}$

**Table 1:** Results for the order  $p^4$  counterterms  $\text{Re } \tilde{K}_i$  from the fit to data done in [13]. The values of  $\text{Re } \tilde{K}_i$  which do not appear are zero. For definitions of the counterterms, see [5, 9].

## B. FSI at NLO for Neutral Kaon Decays: Two-Pion Cuts

Here we include the analytical results for the two-pion cuts contributions to the dispersive part of the neutral decay amplitudes at NLO in CHPT, i.e.  $\mathcal{O}(p^6)$ , coming from diagrams in Figure 6-7. Analogous results for the charged decay amplitudes as well as a more detailed description of the method, based on the use of the optical theorem, can be found in Appendix E of the first reference in [5]. The fully NLO FSI are completed by the calculation of the three-pion cut contributions, whose analytical results are given in Appendix C. In Subsections B.2, B.3 and B.4 we give the dispersive part of the amplitudes  $A_i$  for  $K_{L,S} \rightarrow 3\pi$  denoted by  $\text{Im } A_i^6$  where used the super-index 6 to indicate the CHPT order.

### B.1 Notation

In all the definitions and results written in this Appendix and in Appendices B.2, B.3 and B.4, the functions  $M_i$  and  $P_i$  are only the real part of the corresponding functions  $M_i$  and  $P_i$  defined in [9] and [8] respectively. The expressions in Eqs. (B.9)-(B.25) are thus real.

We define

$$\begin{aligned} \widetilde{M}_i(s) &= \int_{-1}^1 dx \ M_i(a(s) + b(s)x)|_{p^4}, \\ \widetilde{M}_i^s(s) &= \int_{-1}^1 dx \ (a(s) + b(s)x) M_i(a(s) + b(s)x)|_{p^4}, \end{aligned}$$

$$\widetilde{M}_i^{ss}(s) = \int_{-1}^1 dx \ (a(s) + b(s)x)^2 M_i(a(s) + b(s)x) \Big|_{p^4}, \quad (\text{B.1})$$

$$\begin{aligned} \text{with} \quad a(s) &= \frac{1}{2}(3s_0 - s) + \frac{(m_K^2 - m_{\pi^{(3)}}^2)(m_{\pi^{(1)}}^2 - m_{\pi^{(2)}}^2)}{2s}, \\ \text{and} \quad b(s) &= \frac{1}{2s} \left\{ \left[ (s - (m_{\pi^{(2)}} + m_{\pi^{(1)}})^2)(s - (m_{\pi^{(1)}} - m_{\pi^{(2)}})^2) \right] \times \right. \\ &\quad \left. \times \left[ (s - (m_K + m_{\pi^{(3)}})^2)(s - (m_K - m_{\pi^{(3)}})^2) \right] \right\}^{1/2} \end{aligned} \quad (\text{B.2})$$

for  $s = (k - p_3)^2$ , see (2.1).

The amplitudes at  $\mathcal{O}(p^4)$  for the  $\pi\pi \rightarrow \pi\pi$  scattering in a theory with three flavors can be found in [8]. We decompose the amplitudes in the various cases as follows. For the case  $\pi^+\pi^+ \rightarrow \pi^+\pi^+$  the amplitude at  $\mathcal{O}(p^4)$  is

$$\Pi_1 = P_1(s) + P_2(s, t) + P_2(s, u). \quad (\text{B.3})$$

For the case  $\pi^0\pi^0 \rightarrow \pi^+\pi^-$  the amplitude at  $\mathcal{O}(p^4)$  is

$$\Pi_2 = P_3(s) + P_4(s, t) + P_4(s, u). \quad (\text{B.4})$$

For the case  $\pi^+\pi^- \rightarrow \pi^+\pi^-$  the amplitude at  $\mathcal{O}(p^4)$  is

$$\Pi_3 = P_5(s) + P_6(s, t) + P_6(s, u) + P_7(s, t) - P_7(s, u). \quad (\text{B.5})$$

Finally, the amplitude  $\pi^0\pi^0 \rightarrow \pi^0\pi^0$  at  $\mathcal{O}(p^4)$  is

$$\Pi_4 = P_8(s) + P_8(t) + P_8(u). \quad (\text{B.6})$$

The value for the various  $P_i$  can be deduced from [8]. In the following we use

$$\begin{aligned} \widetilde{P}_i^{(n,m)}(s) &= s^n c(s)^m \int_{-1}^1 dx \ (1-x)^m P_i(s, c(s)(1-x)), \\ \hat{P}_{1,i}^{(n)}(s) &= c(s)^n \int_{-1}^1 dx \ (1-x)^n P_i(c(s)(1+x), c(s)(1-x)), \\ \hat{P}_{2,i}^{(n)}(s) &= c(s)^n \int_{-1}^1 dx \ (1-x)^n P_i(c(s)(1-x), s), \end{aligned} \quad (\text{B.7})$$

$$\text{with} \quad c(s) = \frac{1}{2}(4m_\pi^2 - s). \quad (\text{B.8})$$

## B.2 FSI for $K_L \rightarrow \pi^0\pi^0\pi^0$ at NLO

Diagrams A –two charged pions in the loop– and B –two neutral pions in the loop– in Figure 6 correspond to the two possible contributions for  $K_L \rightarrow \pi^0\pi^0\pi^0$ . We first compute the case when the weak vertex in Figure 6 is of  $\mathcal{O}(p^4)$  and the strong vertex of  $\mathcal{O}(p^2)$ . The results are

$$\begin{aligned} \text{Im}A_W^{(6,1)}(s_1, s_2, s_3) &= \text{Im}A_W^{(6,1)}(s_1) + \text{Im}A_W^{(6,1)}(s_2) + \text{Im}A_W^{(6,1)}(s_3), \\ \text{Im}A_W^{(6,1)}(s) &= \frac{\sigma(s)}{16\pi f_\pi^2} (s - m_\pi^2) \left[ M_1(s) + \widetilde{M}_2(s) + \widetilde{M}_3(s)(m_K^2 + 3m_\pi^2 - 2s) \right] \end{aligned}$$

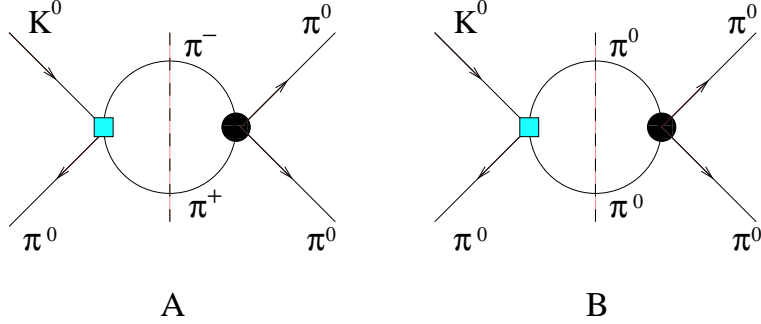


**Figure 6:** Diagrams for the calculation of FSI for  $K_L \rightarrow \pi^0 \pi^0 \pi^0$  using the optical theorem. The square is the weak vertex and the circle is the strong one.

$$- \widetilde{M}_3^s(s) \Big]_{\mathcal{O}(p^4)} \quad (B.9)$$

$$\begin{aligned} \text{Im}A_W^{(6,2)}(s_1, s_2, s_3) &= \text{Im}A_W^{(6,2)}(s_1) + \text{Im}A_W^{(6,2)}(s_2) + \text{Im}A_W^{(6,2)}(s_3), \\ \text{Im}A_W^{(6,2)}(s) &= \frac{\sigma(s)}{32\pi f_\pi^2} m_\pi^2 \left[ M_0(s) + \widetilde{M}_0(s) \right]_{\mathcal{O}(p^4)}. \end{aligned} \quad (B.10)$$

Then we consider the same diagrams of Figure 6 with a weak vertex of  $\mathcal{O}(p^2)$  and a strong vertex of  $\mathcal{O}(p^4)$ . We have

$$\begin{aligned} \text{Im}A_\pi^{(6,1)}(s_1, s_2, s_3) &= \text{Im}A_\pi^{(6,1)}(s_1) + \text{Im}A_\pi^{(6,1)}(s_2) + \text{Im}A_\pi^{(6,1)}(s_3), \\ \text{Im}A_\pi^{(6,2)}(s) &= \frac{\sigma(s)}{16\pi} (M_1(s) + M_3(s)(m_K^2 + m_\pi^2 - 3s)) \Big|_{p^2} (P_3(s) + \widetilde{P}_4^{(0,0)}(s)), \\ \text{Im}A_\pi^{(6,2)}(s_1, s_2, s_3) &= \text{Im}A_\pi^{(6,2)}(s_1) + \text{Im}A_\pi^{(6,2)}(s_2) + \text{Im}A_\pi^{(6,2)}(s_3), \\ \text{Im}A_\pi^{(6,2)}(s) &= \frac{\sigma(s)}{32\pi} (M_0(s_3) + M_0(s_1) + M_0(s_2)) \Big|_{p^2} (P_8(s) + \widetilde{P}_8^{(0,0)}(s)), \end{aligned} \quad (B.11)$$

for those diagrams with two charged and two neutral pions in the loop respectively.

### B.3 FSI for $K_L \rightarrow \pi^+ \pi^- \pi^0$ at NLO

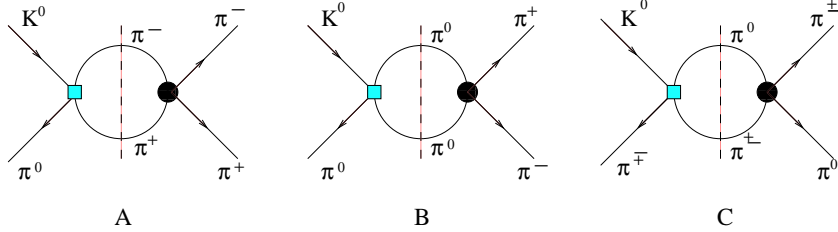


**Figure 7:** Diagrams for the calculation of FSI for  $K_L \rightarrow \pi^+ \pi^- \pi^0$  using the optical theorem. The square is the weak vertex and the circle is the strong one.

The calculation is analogous to the one for  $K_L \rightarrow \pi^0 \pi^0 \pi^0$ . The three contributions in Figure 7 correspond to two charged pions in the loop –results in Eqs. (B.12) and (B.16), two neutral pions in the loop –results in Eqs. (B.13) and (B.17)– and loops with one neutral and one charged pions. In the last case we have a S-wave contribution –results in

(B.14) and (B.18), and a P-wave contribution –results in (B.15) and (B.19), respectively. Eqs. (B.12), (B.13), (B.14), and (B.15) are the results of using the weak vertex at  $\mathcal{O}(p^4)$  and the strong vertex at  $\mathcal{O}(p^2)$ . Eqs. (B.16), (B.17), (B.18), and (B.19) are the results of using the weak vertex at  $\mathcal{O}(p^2)$  and the strong vertex at  $\mathcal{O}(p^4)$ .

$$\text{Im}A_W^{(6,1)} = \frac{\sigma(s_3)}{16\pi f_\pi^2} (s_3) \left[ M_1(s_3) + \widetilde{M}_2(s_3) + \widetilde{M}_3(s_3)(m_K^2 + 3m_\pi^2 - 2s_3) - \widetilde{M}_3^s(s_3) \right]_{\mathcal{O}(p^4)}, \quad (\text{B.12})$$

$$\text{Im}A_W^{(6,2)} = \frac{\sigma(s_3)}{32\pi f_\pi^2} (s_3 - m_\pi^2) \left[ M_0(s_3) + \widetilde{M}_0(s_3) \right]_{\mathcal{O}(p^4)}, \quad (\text{B.13})$$

$$\text{Im}A_{W,S}^{(6,3)} = \frac{\sigma(s_1)}{32\pi f_\pi^2} (m_\pi^2 - s_1/2) \left[ 2M_2(s_1) + \widetilde{M}_2(s_1) + \widetilde{M}_1(s_1) - \widetilde{M}_3(s_1)(m_K^2 + 3m_\pi^2 - 2s_1) + \widetilde{M}_3^s(s_1) \right]_{\mathcal{O}(p^4)} + s_1 \leftrightarrow s_2, \quad (\text{B.14})$$

$$\begin{aligned} \text{Im}A_{W,P}^{(6,3)} = & \frac{\sigma(s_1)}{64\pi f_\pi^2} \frac{s_1(s_2 - s_3)}{s_1^2 - 2s_1(m_K^2 + m_\pi^2) + (m_K^2 - m_\pi^2)^2} \\ & \times \left[ (s_1 - m_K^2 - 3m_\pi^2)(\widetilde{M}_2(s_1) - \widetilde{M}_1(s_1)) \right. \\ & + (2s_1 - m_K^2 - 3m_\pi^2)\widetilde{M}_3(s_1)) + (2\widetilde{M}_2^s(s_1) - 2\widetilde{M}_1^s(s_1) \\ & \left. + (5s_1 - 3m_K^2 - 9m_\pi^2)\widetilde{M}_3^s(s_1)) + 2\widetilde{M}_3^{ss}(s_1) + \frac{8}{3}b(s_1)^2 M_3(s_1) \right]_{\mathcal{O}(p^4)} \\ & + s_1 \leftrightarrow s_2. \end{aligned} \quad (\text{B.15})$$

$$\text{Im}A_\pi^{(6,1)} = \frac{\sigma(s_3)}{16\pi} (M_1(s_3) + M_3(s_3)(m_K^2 + 3m_\pi^2 - 3s_3))|_{p^2} (P_5(s_3) + \widetilde{P}_6^{(0,0)}(s_3)), \quad (\text{B.16})$$

$$\text{Im}A_\pi^{(6,2)} = \frac{\sigma(s_3)}{32\pi} (M_0(s_3) + M_0(s_1) + M_0(s_2))|_{p^2} (P_3(s_3) + \widetilde{P}_4^{(0,0)}(s_3)), \quad (\text{B.17})$$

$$\begin{aligned} \text{Im}A_{\pi,S}^{(6,3)} = & \frac{\sigma(s_1)}{32\pi} \left( M_1(s_1) + \frac{1}{2}M_3(s_2)(s_1 - s_3) + \frac{1}{2}M_3(s_3)(s_1 - s_2) \right)|_{p^2} \\ & \times \left( \widetilde{P}_3^{(0,0)}(s_1) + \hat{P}_{1,4}^{(0)}(s_1) + \widetilde{P}_{2,4}^{(0)}(s_1) \right) + s_1 \leftrightarrow s_2 \end{aligned} \quad (\text{B.18})$$

$$\begin{aligned} \text{Im}A_{\pi,P}^{(6,3)} = & \frac{\sigma(s_1)}{64\pi} (3M_3(s_1)(s_2 - s_3))|_{p^2} \frac{1}{s_1 - 4m_\pi^2} \\ & \times \left( (s_1 - 4m_\pi^2)(\widetilde{P}_3^{(0,0)}(s_1) - \hat{P}_{1,4}^{(0)}(s_1) + \widetilde{P}_{2,4}^{(0)}(s_1)) + 2\widetilde{P}_3^{(1,0)}(s_1) \right. \\ & \left. - 2\widetilde{P}_{1,4}^{(1)}(s_1) + 2\hat{P}_{2,4}^{(1)}(s_1) \right) + s_1 \leftrightarrow s_2. \end{aligned} \quad (\text{B.19})$$

#### B.4 FSI for $K_S \rightarrow \pi^+ \pi^- \pi^0$ at NLO

The diagrams contributing to this decay are the same depicted in Figure 7. The result corresponding to diagram A in Figure 7 is in Eq. B.20 for the weak vertex at  $\mathcal{O}(p^4)$  and the strong vertex at  $\mathcal{O}(p^2)$  and in Eq. B.23 for the weak vertex at  $\mathcal{O}(p^2)$  and the strong vertex at  $\mathcal{O}(p^4)$ . In this case there is only P-wave contribution.

Diagram B in Figure 7 does not contribute. Diagram C in Figure 7 gives both an S-wave – results in Eqs. (B.21) and (B.24) – and a P-wave contribution – results in (B.22) and (B.25). Equations (B.21) and (B.22) are the results of the case in which the weak vertex is at  $\mathcal{O}(p^4)$  and strong vertex at  $\mathcal{O}(p^2)$  in diagram C. Equations (B.24) and (B.25) are the results for the case in which the weak vertex is at  $\mathcal{O}(p^2)$  and the strong vertex at  $\mathcal{O}(p^4)$  in diagram C.

$$\text{Im}A_{W,P}^{(6,1)} = \frac{\sigma(s_3)}{16\pi f_\pi^2} \frac{s_3(s_1 - s_2)}{s_3^2 - 2(m_K^2 + m_\pi^2)s_3 + (m_K^2 - m_\pi^2)^2} \left\{ a(s_3)(\widetilde{M}_4(s_3) + (2a(s_3) - s_3)\widetilde{M}_5(s_3)) - (\widetilde{M}_4^s(s_3) + (3a(s_3) - s_3)\widetilde{M}_5^s(s_3)) + \widetilde{M}_5^{ss}(s_3) - \frac{2}{3}b(s_3)^2 M_6(s_3) \right\} \quad (\text{B.20})$$

$$\text{Im}A_{W,S}^{(6,2)} = \frac{\sigma(s_1)}{64\pi f_\pi^2} (2m_\pi^2 - s_1) \left\{ 2M_4(s_1) - \widetilde{M}_4(s_1) + (m_K^2 + 3m_\pi^2 - 2s_1)(\widetilde{M}_5(s_1) - \widetilde{M}_6(s_1)) - \widetilde{M}_5^s(s_1) + \widetilde{M}_6^s(s_1) \right\} - s_1 \leftrightarrow s_2, \quad (\text{B.21})$$

$$\begin{aligned} \text{Im}A_{W,P}^{(6,2)} = & \frac{\sigma(s_1)}{32\pi f_\pi^2} \frac{s_1(s_3 - s_2)}{s_1^2 - 2s_1(m_K^2 + m_\pi^2) + (m_K^2 - m_\pi^2)} \\ & \times \left\{ \frac{4}{3}b(s_1)^2 M_5(s_1) + a(s_1)(\widetilde{M}_4(s_1) - (2a(s_1) - s_1)(\widetilde{M}_5(s_1) + \widetilde{M}_6(s_1))) \right. \\ & \left. - \widetilde{M}_4^s(s_1) + (3a(s_1) - s_1)(\widetilde{M}_5^s(s_1) + \widetilde{M}_6^s(s_1)) - \widetilde{M}_5^{ss}(s_1) - \widetilde{M}_6^{ss}(s_1) \right\} \\ & - s_1 \leftrightarrow s_2 \end{aligned} \quad (\text{B.22})$$

$$\text{Im}A_{\pi,P}^{(6,1)} = -\frac{\sigma(s_3)}{16\pi} \frac{(M_4(s_1) - M_4(s_2))|_{p^2}}{s_3 - 4m_\pi^2} \left[ (s_3 - 4m_\pi^2)\widetilde{P}_7^{(0,0)}(s_3) + 2\widetilde{P}_7^{(0,1)}(s_3) \right], \quad (\text{B.23})$$

$$\begin{aligned} \text{Im}A_{\pi,S}^{(6,2)} = & \frac{\sigma(s_1)}{64\pi} M_5(s_1)|_{p^2} (3s_1 - (m_K^2 + 3m_\pi^2))(\widetilde{P}_3^{(0,0)}(s_1) + \widetilde{P}_{2,4}^{(0)}(s_1) \\ & + \widetilde{P}_{1,4}^{(0)}(s_1)) - s_1 \leftrightarrow s_2, \end{aligned} \quad (\text{B.24})$$

$$\begin{aligned} \text{Im}A_{\pi,P}^{(6,2)} = & \frac{\sigma(s_1)}{64\pi} (M_4(s_2) - M_4(s_3))|_{p^2} \frac{1}{s_1 - 4m_\pi^2} \\ & \times \left( (s_1 - 4m_\pi^2)(\widetilde{P}_3^{(0,0)}(s_1) - \hat{P}_{1,4}^{(0)}(s_1) + \widetilde{P}_{2,4}^{(0)}(s_1)) + 2\widetilde{P}_3^{(1,0)}(s_1) \right. \\ & \left. - 2\widetilde{P}_{1,4}^{(1)}(s_1) + 2\hat{P}_{2,4}^{(1)}(s_1) \right) - s_1 \leftrightarrow s_2. \end{aligned} \quad (\text{B.25})$$

### C. Three-Pion Cut Contributions to FSI

To calculate the contributions of the topologies in Figure 1 B,C and D to the FSI, we need the tree level vertices of  $K \rightarrow 3\pi$  and  $3\pi \rightarrow 3\pi$ . The complete tree level amplitude of the  $3\pi \rightarrow 3\pi$  scattering can be easily calculated using the code **Ampcalculator** developed in [24]. In this way all possible  $3\pi \rightarrow 3\pi$  are included. In order to perform the integral in the phase space as prescribed in the optical theorem we assign the momentum to pions as

shown in an example in Figure 8. The momentum assignment is done preserving the suffix 3 for the *odd* pion in the  $K^+ \rightarrow 3\pi$  vertex.

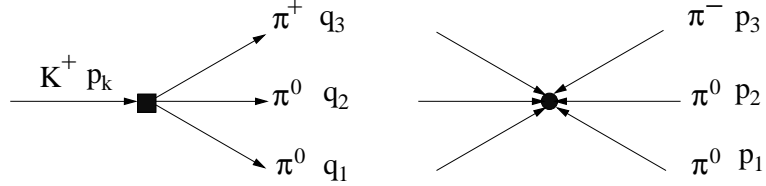


**Figure 8:** Example of diagram for the calculation of FSI for  $K^+ \rightarrow \pi^0\pi^0\pi^+$  with momentum assignment.

In order to perform the integral in the phase space over momentum  $q_i$  it is necessary to fix a reference frame. We chose the reference frame in which the decaying kaon is at rest and the momentum  $p_3$  defines the z-axis,

$$\begin{aligned} p_K &= (M_K, 0, 0, 0), & p_3 &= (p_3^0, 0, 0, \bar{p}_3), & p_1 &= (p_1^0, 0, \bar{p}_1 \sin \eta, \bar{p}_1 \cos \eta), \\ p_2 &= -p_K - p_1 - p_3. \end{aligned} \quad (C.1)$$

The momenta  $q_i$  describe also a decay of a kaon into three pions. The most general expression for these momenta, in the chosen reference frame, is

$$\begin{aligned} q_i &= R_z(\alpha)R_y(\beta)R_z(\gamma) r_i, \\ r_3 &= (r_3^0, 0, 0, \bar{r}_3), & r_1 &= (r_1^0, 0, \bar{r}_1 \sin \theta, \bar{r}_1 \cos \theta), & r_2 &= p_K - r_1 - r_3, \end{aligned}$$

and  $R_{z(y)}(\delta)$  are rotations around axis  $z$  ( $y$ ) with Euler angle  $\delta$ . Using the Particle Data Group (PDG) parametrization for the phase space integrals [25], the LO contribution to  $\text{Im}\bar{A}_{00+}$  and  $\text{Im}\bar{B}_{00+}$  of the 3-pion cut diagrams so read

$$\begin{aligned} \text{Im}\bar{A}_{00+}^{3\pi,LO}(s_1, s_2, s_3) &= \frac{1}{16(2\pi)^5} \int dq_3^0 dq_2^0 d\alpha d\cos\beta d\gamma \left[ A_{00+}^{(p^2)}(p_K, q_i) A_{3\pi,0}^{(p^2)}(q_i, p_i) \right], \\ v_{\pm} \text{Im}\bar{B}_{00+}^{3\pi,LO}(s_1, s_2, s_3) &= \frac{1}{16(2\pi)^5} \int dq_3^0 dq_2^0 d\alpha d\cos\beta d\gamma \left[ A_{++-}^{(p^2)}(p_K, q_i) A_{3\pi,\pm}^{(p^2)}(q_i, p_i) \right], \end{aligned} \quad (C.2)$$

where  $A_{3\pi,0}^{(p^2)}(q_i, p_i)$ ,  $A_{3\pi,\pm}^{(p^2)}(q_i, p_i)$  are the tree level amplitudes for  $\pi^0\pi^0\pi^+ \rightarrow \pi^0\pi^0\pi^+$  and  $\pi^+\pi^+\pi^- \rightarrow \pi^0\pi^0\pi^+$ . At this order there are no contribution of these topologies to  $\text{Re}\bar{B}_{00+}$ . We have computed numerically the integrals in (C.2). The correction induced by (C.2) to the other LO terms is always much below the 0.5%. We find so perfectly consistent to omit these corrections at this level of precision. Similar expressions and conclusions hold for the FSI in the decay of  $K_L \rightarrow \pi^0\pi^0\pi^0$ . For this case one has just

$$\begin{aligned} \text{Im}\bar{A}_{000}^{3\pi,LO}(s_1, s_2, s_3) &= \frac{1}{16(2\pi)^5} \int dq_3^0 dq_2^0 d\alpha d\cos\beta d\gamma \left[ A_{000}^{(p^2)}(p_K, q_i) \tilde{A}_{3\pi,0}^{(p^2)}(q_i, p_i) \right], \\ v_{\pm} \text{Im}\bar{B}_{000}^{3\pi,LO}(s_1, s_2, s_3) &= \frac{1}{16(2\pi)^5} \int dq_3^0 dq_2^0 d\alpha d\cos\beta d\gamma \left[ A_{+-0}^{(p^2)}(p_K, q_i) \tilde{A}_{3\pi,\pm}^{(p^2)}(q_i, p_i) \right], \end{aligned} \quad (C.3)$$

where  $\tilde{A}_{3\pi,0}^{(p^2)}(q_i, p_i)$ ,  $\tilde{A}_{3\pi,\pm}^{(p^2)}(q_i, p_i)$  are the tree level amplitudes for  $\pi^0\pi^0\pi^0 \rightarrow \pi^0\pi^0\pi^0$  and  $\pi^+\pi^-\pi^0 \rightarrow \pi^0\pi^0\pi^0$ .

## References

- [1] G. Ecker, hep-ph/0011026; A. Pich, hep-ph/9806303.
- [2] G. Ecker, Prog. Part. Nucl. Phys. **35** (1995) 1; E. de Rafael, hep-ph/9502254; A. Pich, Rept. Prog. Phys. **58** (1995) 563.
- [3] S. Weinberg, Physica **A 96** (1979) 327.
- [4] J. Gasser and H. Leutwyler, Annals Phys. **158** (1984) 142; Nucl. Phys. **B 250** (1985) 465.
- [5] E. Gámiz, J. Prades and I. Scimemi, J. High Energy Phys. **10** (2003) 042; hep-ph/0410150; hep-ph/0305164.
- [6] I. Scimemi, E. Gámiz and J. Prades, Proc. of the 39<sup>th</sup> Rencontres de Moriond on Electroweak Interactions and Unified Theories, p. 355, The Gioi Publishers (2005), hep-ph/0405204.
- [7] J. Prades, E. Gámiz and I. Scimemi, Proc. of QCD'05, Montpellier, 4-8 July 2005, hep-ph/0509346.
- [8] V. Bernard, N. Kaiser and U.-G. Meißner, Nucl. Phys. **B 357** (1991) 129.
- [9] J. Bijnens, P. Dhonte and F. Persson, Nucl. Phys. **B 648** (2003) 317.
- [10] J. Kambor, J. Missimer and D. Wyler, Nucl. Phys. **B 346** (1990) 17; Phys. Lett. **B 261** (1991) 496.
- [11] J. Kambor, J.F. Donoghue, B.R. Holstein, J. Missimer and D. Wyler, Phys. Rev. Lett. **68** (1992) 1818.
- [12] J. Bijnens and F. Borg, Nucl. Phys. **B 697** (2004) 319; Eur. Phys. J. **C 39** (2005) 347; A. Nehme, Phys. Rev. **D 70** (2004) 094025.
- [13] J. Bijnens and F. Borg, Eur. Phys. J. **C 40** (2005) 383.
- [14] N. Cabibbo, Phys. Rev. Lett. **93** (2004) 121801.
- [15] U.-G. Meißner, G. Müller and S. Steininger, Phys. Lett. B **406** (1997) 154 [Erratum-ibid. B **407** (1997) 454].
- [16] N. Cabibbo and G. Isidori, J. High Energy Phys. **03** (2005) 021.
- [17] G. D'Ambrosio, G. Isidori, A. Pugliese and N. Paver, Phys. Rev. D **50** (1994) 5767 [Erratum-ibid. D **51** (1995) 3975].
- [18] J.R. Batley *et al.* [NA48/2 Collaboration], Phys. Lett. **B 633** (2006) 173; S. Giudici [NA48/2 Collaboration], hep-ex/0505032.
- [19] J. Gasser, Talk at IV EURIDICE Collaboration Meeting, Marseille 8-11 February 2006.
- [20] G. Colangelo, J. Gasser and H. Leutwyler, Phys. Lett. **B 488** (2000) 261, Nucl. Phys. **B 603** (2001) 125.
- [21] J.R. Peláez and F.J. Ynduráin, Phys. Rev. **D 71** (2005) 074016; hep-ph/0412320.
- [22] J. Gasser, private communication; G. Colangelo, J. Gasser, B. Kubis, and A. Rusetsky, in preparation.
- [23] A.V. Anisovich, Phys. Atom. Nucl. **66** (2003) 172 [Yad. Fiz. **66** (2003) 175]; V.V. Anisovich and A.A. Ansel'm, Usp. Fiz. Nauk. **88** (1966) 287 [Sov. Phys. Usp. **9** (1966) 117].
- [24] R. Unterdorfer and G. Ecker, J. High Energy Phys. **10** (2005) 017.
- [25] S. Eidelman *et al.* [Particle Data Group], Phys. Lett. **B 592** (2004) 1.